This is a post-peer-review, pre-copyedit version of an article published in the journal "Applied Ocean Research" (Elsevier).
The final authenticated version is available online at https://doi.org/10.1016/j.apor.2018.09.013.

Improved relaxation zone method in SPH-based model for coastal engineering applications

C. Altomare[1,2,*], B. Tagliafierro[3], J. M. Dominguez[4], T. Suzuki[1,5], G. Viccione[3]

[1]Flanders Hydraulics Research, Berchemlei 115, 2140 Antwerp, Belgium

[2]Ghent University, Department of Civil Engineering, Technologiepark 904, 9000 Ghent, Belgium

[3]University of Salerno, Dept. of Civil Engineering, Via Giovanni Paolo II, 132, 84084 Fisciano (SA), Italy

[4]EPHYSLAB, Vigo University, AS Lagoas, 32004 Ourense, Spain

[5] Faculty of Civil Engineering and Geosciences, Delft University of Technology, Stevinweg 1, 2628 CN Delft, The Netherlands

*Corresponding author. Tel: +32-32246154; Email address: corrado.altomare@mow.vlaanderen.be (C. Altomare)

Abstract
An improved Relaxation Zone (RZ) method has been implemented in the meshless SPH-based DualSPHysics model. Final purpose of this work is to have a general wave generation scheme that allows coupling SPH-based models to other models, e.g. Eulerian based wave models, besides employing the RZ as alternative wave generation in SPH as a stand-alone scheme. Using RZ in SPH, the movement of the fluid particles is controlled by correcting their orbital velocity by means of a weighting function in a specified generation area. In the present work, the new technique is used to couple DualSPHysics to the non-hydrostatic wave-flow model SWASH. The results of RZ employed both as stand-alone wave generation technique and as coupling framework with SWASH model are validated for wave generation and wave reflection for monochromatic waves. Then, the method is tested successfully for generation and absorption of irregular waves. Finally, the coupling between DualSPHysics and SWASH using RZ is validated against experimental data concerning the wave flow impacts on vertical walls. A procedure for a proper design of the RZ (i.e. shape of the weighting function, size of the RZ) is described in the present work. Overall, the results indicate that the proposed improved RZ technique is among the most effective alternatives for wave generation in SPH-based models for coastal engineering application.

Keywords: Smoothed Particle Hydrodynamics; Relaxation Zone; Coupling algorithm; Wave generation and absorption; SWASH; Wave-Structure interaction.

1 Introduction

Meshless methods are getting popular in coastal engineering as result of the developments of numerical techniques and computation technologies in the last decades and are more and more often employed to study free-surface flows and wave-structure interaction phenomena [1]. Models based on the so-called Smoothed Particle Hydrodynamics (SPH) [2,3] method are becoming very popular among researchers for their capacity to simulate highly nonlinear free-surface flows (e.g. [4]). However the computational cost of the SPH models is still huge, even compared with one of the most expensive wave models, e.g. RANS-VOF models [5]. In particular, one of the SPH models, namely DualSPHysics [6], significantly improved the computational time by using GPU (Graphics Processing Unit) and multi-GPU techniques [7,8], although the computational cost is still high and thus it is not always easy to apply it to realistic coastal engineering projects.

In order to overcome this limitation, a coupling to computationally less demanding wave models was introduced and proved to be useful for coastal engineering applications, as for example in [9]. On the one hand, less demanding computational models (e.g. Boussinesq models, Non-Linear Shallow Water equation models) are accurate enough for wave transformation at a reasonable computational cost but not very accurate for wave-structure interaction due to their assumptions (e.g. depth integrated feature). On the other hand, SPH models are capable of generating accurate results for both wave transformation and wave-structure interaction [10,11] while these are computationally too expensive to cover a large domain at affordable time duration.

Coupling to other models is actually identified as one of the SPHERIC Grand Challenges from the Ercoftac Special Interest Group for SPH (SPHERIC, http://spheric-sph.org/). More and more attempts to enhance the SPH capability of modelling real engineering problems by means of coupling techniques have been presented during the last years (e.g. [12,13]). Previous attempts to couple DualSPHysics with wave propagation models can be found in [14,15]. In [14] SWASH model is hybridized with DualSPHysics. SWASH is a model based on layer-averaged Non-Linear Shallow Water equations with non-hydrostatic pressure and is much less demanding computationally. The wave propagation is calculated by SWASH and wave-structure interaction is calculated by DualSPHysics. In this way, the drawbacks of each model are overcome. Waves are generated in DualSPHysics by means of moving boundaries that move accordingly to the velocity input from SWASH. However, the displacement of the moving boundary in DualSPHysics does not take into account any compensation for the reflected waves that might reach the generation zone: therefore, this method does not allow wave generation over longer time periods. This problem is solved by activating AWAS (Active Wave Absorption System) at the wave generation [16] in DualSPHysics used as stand-alone model, but there is no similar implementation for the coupled model. In [15] a two-way coupling methodology between a fully nonlinear potential flow wave propagation model and DualSPHysics was introduced. Boundary moving blocks are used in DualSPHysics to generate and absorb waves. However, there are two main limitations in the methodology proposed by [15]: i) the vertical orbital velocities are not coupled; ii) the horizontally moving boundaries slowly drift away from each other, limiting the simulation time. All the three approaches ([14–16]) implement moving boundaries (hereafter MB) mimicking piston-type wavemakers for generating waves in SPH. Therefore, the implementations are rather different with respect to the RZ method here presented, which prevents the use of moving boundaries. The differences are following described:

- In [14] the MB real time displacement is reconstructed on the basis of the velocity time series calculated by SWASH model in a specific point of the fluid domain: the method, even though very efficient and accurate to study phenomena such as wave run-up on gentle beaches, has a strong limitation for highly reflective cases. In fact, re-reflection at the MB is not prevented, limiting the application of the technique to low-reflective cases or to a very short time series. Instead, RZ technique allows a coupling where the reflected waves are compensated inside the relaxation zone. In this way, both highly reflective cases and long wave time series can be generated, without biasing the results for extra spurious wave energy introduced in the system by wave re-reflection.
- In [15] the MB is discretized in moving blocks that move only horizontally and the movement of which can generate a drift. The drift will cause detachment of one block with the contiguous one which is only prevented by limiting the simulation in time.
- In [16] the MB mimics an experimental piston-type wavemaker with reflection compensation employing the correction proposed by [17] based on shallow-water linear theory. It is a pure wave generation and absorption technique, to be used only in DualSPHysics as stand-alone model. Instead, the RZ method can be employed as coupling framework between the DualSPHysics model and a wave propagation model (e.g. SWASH).

To summarize, [16] presented a wave generation technique in SPH with no coupling, meanwhile [14] described the implementation of a coupling based on MB which lacks of active wave absorption system to prevent wave re-reflection. Instead, a coupled model between DualSPHysics and SWASH with reflection compensation seems to be a promising model for coastal engineering application but still there is a

limitation for shallow foreshore applications (e.g. [18,19]). In principle the coupling point should be outside the breaking zone since AWAS is based on the linear theory and thus it could only be applied to non-breaking area where non-linear effects are limited. Ideally the coupling point is placed as close to the target structure as possible. This indicates that the coupling point for the shallow foreshore case (where the distance between coastal structures and breaking zone is big) needs to be in the breaking zone, otherwise the efficiency of the coupling model is limited.

As seen above for a specific hybridization between DualSPHysics and SWASH, the coupling between the two numerical models relies on the method used to transfer information from one model to another and on the technique that each model implements to generate sea waves but also to absorb wave reflection. In particular, three kinds of wave generation techniques can be identified for numerical wave tanks [20]: MB wave generation, static-boundary and internal wave generation. The first mechanism mimics the wave generation as in experimental facilities, implementing a moving boundary as a numerical wave-maker that generates and absorbs waves, e.g. [21]. This type of wave generation is ideal for SPH models because of their Lagrangian nature and, hence, has been implemented in DualSPHysics [16]. The second mechanism corresponds to static wave generation and absorption (i.e. Dirichlet-type boundary conditions). Examples include RANS [22,23], NLSW models (e.g. SWASH: [24]) and potential flow models [25]. Examples of internal wave generation exist for RANS [26] and potential flow models [27]. In SPH, Liu et al. [28] proposed a non-reflective internal wavemaker algorithm, where a momentum source term derived from the Boussinesq equations is employed and added into the Lagrangian form of Navier–Stokes equations for an Incompressible SPH model. For Weakly Compressible SPH, [29] presented a momentum source function derived from the linear wave theory. Recently a wave generation method based on the so-called Relaxation Zone (RZ) technique has been introduced in SPH [30]. The authors refer to this approach as "source generation" in SPH. However, this sounds not appropriate since it is basically an application of the RZ to a meshless method. Some very early works having a similar kind of wave generation method can be found in literature, for example for solitary wave generation as presented by [31], where the authors specify the initial wave conditions by applying the analytical solution for wave profile and horizontal wave velocity to the SPH fluid particles. Note that what presented in [30] is different from the method of [32], which actually uses source generation with the boundary integral equation method (BIEM) to generate nonlinear gravity waves in Eulerian methods. Therefore, the approach presented in [30] will be redefined as RZ hereafter. Unlike the source generation with BIEM and MB wave generators such as piston-type wave-makers, RZ is a numerical method in which the movement of the particles is controlled by a weighting function (i.e. C function) in a specified generation domain. Since RZ is a pure numerical method, it might be applied to cases in which MB cannot be used (e.g., sea dikes with very shallow and mild foreshore slopes). A part from the aforementioned wave generation techniques, it is worth to mention the open boundary conditions (OBCs) as a very specific implementation for SPH and meshless methods in general [33,34]. Very recently, [35] proposed a SPH numerical wave flume with wave generation and wave absorption techniques based on the non-reflective open boundary conditions, capable of generating solitary waves, linear and second-order regular waves. Yet, the second-order bound long wave generation and active wave absorption of irregular waves was not considered in [35].

The aim of the present work is to validate a revised RZ technique which moves beyond [30], by implementing the concept in DualSPHysics with relevant improvements. In fact, even though [30] introduced the RZ in the SPH-based models, it is limited only to regular waves, whereas random waves (i.e. real sea states) are not modelled. Furthermore, the accuracy of the method is not assessed in case of highly reflective wave conditions, which always represent the most critical situation to judge the performance of a wave generation and absorption techniques, either in a numerical scheme or an experimental set up. Hence, the RZ has been improved and optimized with respect to the one proposed in [30] as follows:

i) the weighting function C has been re-defined in a more general way, assuming a hyperbolic functional, the shape of which can be varied depending on the case study;
ii) the effectiveness of the C function has been analyzed in depth with reference to wave generation and wave absorption;

iii) a method to design the RZ has been established and it is proposed in this work; a drift correction is introduced to compensate the mass transport as predicted by Stokes' 2nd order solution in order to avoid the unphysical decrease of the water level in the RZ;
iv) the RZ has been extended to study test cases characterized by highly reflective conditions;
v) the RZ has been validated not only for monochromatic waves as in [30] but also for irregular waves;
vi) finally, the RZ technique has been applied for coupling DualSPHysics with a less computational-expensive wave propagation model, such as SWASH.

In this work the applicability and the limitations of this method for wave transformation and wave reflection compensation are discussed. To this end, we define a geometrical layout that includes a highly reflective condition, namely a vertical wall. Once the RZ is validated for DualSPHysics as stand-alone model, the method is extended to the coupling case to SWASH, and the basic behavior is investigated. Final aim of the work is, in fact, to employ RZ not only as internal wavemaker in DualSPHysics where other wave generation techniques fails, but also and most of all as a mean to couple SPH models to Eulerian grid-based methods. Despite some attempts to enhance the SPH capability of modelling engineering problems by means of coupling techniques, the present work comprehensively analyze the performance of the coupling technique for real engineering cases and different wave conditions.

2 Numerical models

2.1 The SPH-based DualSPHysics model

Smoothed Particle Hydrodynamics is a fully Lagrangian and meshless method [3], where the fluid is discretised into a set of particles or nodal points. Physical quantities of each particle, such as position, velocity, density and pressure, are computed as an interpolation of the values of the neighbouring particles. The contribution of the nearest particles is computed depending on the distance between particles and using a weighted kernel function (W). The area of influence of the kernel function is defined using a characteristic length called smoothing length (h_{SPH}). In addition, the kernel presents compact support to avoid contributions with other particles beyond that distance. In general, SPH methods can be grouped into two main categories: Weakly Compressible and Incompressible. Weakly Compressible SPH (WCSPH) methods solve an appropriate equation of state (Tait's equation) in a fully explicit form (e.g. [36]) whereas Incompressible SPH (ISPH) methods solve a Poisson pressure equation by applying project-based methods. A comprehensive review of the latest advancements in the context of WCSPH and ISPH methods in terms of model stability, accuracy, energy conservation, boundary conditions and simulations of multiphase flows and fluid–structure interactions is presented in [1].

The WCSPH DualSPHysics code is used in this work. DualSPHysics [37,6] is an open-source code developed by the University of Vigo (Spain) and the University of Manchester (UK) in collaboration with experts from all around the globe that can be freely downloaded from www.dual.sphysics.org.. The code is written in two languages, namely C++ and CUDA, and optimised to use the parallel processing power of either CPUs and/or GPUs [7], thus making the study of real engineering problems possible [38–40]. In what follows the governing equations implemented in the software are introduced; then, the boundary condition treatment and extra functionalities such as wave generation and absorption are described.

2.1.1 SPH formulation

The discrete SPH Lagrangian system of governing equations of weakly compressible flow, following Monaghan [41], is:

$$\frac{d\rho_a}{dt} = \sum_b m_b (\mathbf{v}_a - \mathbf{v}_b) \nabla_a W_{ab} \tag{1}$$

$$\frac{d\mathbf{v}_a}{dt} = -\sum_b m_b \left(\frac{P_b + P_a}{\rho_b \cdot \rho_a} + \Pi_{ab} \right) \nabla_a W_{ab} + \mathbf{g} \tag{2}$$

$$\frac{d\mathbf{r}_a}{dt} = \mathbf{v}_a \tag{3}$$

being t time, $\mathbf{r}$ position, $\mathbf{v}$ velocity, P pressure, ϱ density, m mass, $\mathbf{g}$=(0,0,-9.81) m·s^{-2} the gravitational acceleration and W_{ab} the kernel function that depends on the distance between particles a and b. The Quintic kernel [42], where the weighting function vanishes for inter-particle distances greater than $2h_{SPH}$, was adopted for the present study. Π_{ab} is the viscous term according to the artificial viscosity proposed in [41]. Besides the most classical diffusion schemes such as the artificial viscosity, DualSPHysics implements the so-called δ-SPH scheme as well, as proposed by [43], in order to increase accuracy of the pressure field.

The system is closed by the addition of Tait's equation of state

$$P = B\left[\left(\frac{\rho}{\rho_0}\right)^{\gamma} - 1\right] \tag{4}$$

where γ=7 is the polytropic constant and $B=c_0^2\rho_0/\gamma$, being ϱ_0 the reference density and c_0 the numerical speed of sound. More details about formulation can be found in [6]. In addition, recently an automatic optimization framework to find the set of SPH parameters in DualSPHysics for an accurate wave propagation modelling was proposed in [44]. Specific parameters that have been used in the simulations presented in this work can be also found in [10].

2.1.2 Boundaries

In the DualSPHysics code, boundaries are described using a discrete set of boundary particles that exert a repulsive force on the fluid particles when they approach the boundary particles. A dynamic boundary condition [45] is used, where the boundary particles satisfy the same equations as the fluid particles; however, they do not move according to the forces exerted on them. Instead, they remain fixed (fixed boundary) or move according to some externally imposed movement (moving boundary such as gates, flaps...). Using this boundary condition, when a fluid particle approaches a boundary particle and the distance between them decreases beyond the kernel range, the density of the boundary particles increases giving rise to an increase in pressure. This results in a repulsive force being exerted on the fluid particle due to the pressure term in the momentum equation.

2.1.3 Wave generation and active wave absorption in DualSPHysics

The implementation of long-crested wave generation and absorption in DualSPHysics as stand-alone model is described and validated in [16]: the waves are generated by means of moving boundaries that aim to mimic the movement of a piston- and flap-type wavemakers as in physical facilities. Both first- and second-order wave generation theories have been implemented. For monochromatic waves that means to include super-harmonics. For random waves, sub-harmonic components (bound long waves) are considered to suppress spurious long waves. Two standard wave spectra are implemented and used to generate random waves: JONSWAP and Pierson-Moskowitz spectra. The generation system allows having different random time series with the same significant wave height (H_{m0}) and the same peak period (T_p), just defining different phase seeds.

To absorb the reflected waves at the wavemaker and prevent the introduction of extra spurious energy in the fluid domain, the so-called Active Wave Absorption System (AWAS) has been implemented in DualSPHysics. The water surface elevation η at the wavemaker position is used and transformed by an appropriate time-domain filter to obtain a control signal that corrects the wave paddle displacement in order to absorb the reflected waves every time step. The position in real time of the wavemaker is obtained through the velocity correction of its motion. Further details on AWAS in DualSPHysics are reported in [16].

2.2 SWASH model

The SWASH model [24] is an open-source non-hydrostatic wave-flow model (available at swash.sourceforge.net). The basic mass and momentum balance of incompressible fluid with a free-surface are implemented. The model can be used in one-layer and in multi-layers. The governing equations for one-layer calculation are the non-linear shallow water equations, including a non-hydrostatic pressure term. The governing equations for multi-layer calculation applied in this study, where the vertical plain is divided into two or more layers, are shown below:

$$\frac{\partial u}{\partial x}+\frac{\partial w}{\partial z}=0 \tag{5}$$

$$\frac{\partial u}{\partial t}+\frac{\partial uu}{\partial x}+\frac{\partial wu}{\partial z}=-\frac{\partial (p_h+p_{nh})}{\partial x}+\frac{\partial \tau_{xz}}{\partial z}+\frac{\partial \tau_{xx}}{\partial x} \tag{6}$$

$$\frac{\partial w}{\partial t}+\frac{\partial uw}{\partial x}+\frac{\partial ww}{\partial z}=-\frac{\partial p_{nh}}{\partial x}+\frac{\partial \tau_{zz}}{\partial z}+\frac{\partial \tau_{zx}}{\partial x} \tag{7}$$

where t is time, x and z are the horizontal and vertical coordinates, u and w are the velocity in x- and z-direction, respectively. p_h and p_{nh} are the hydrostatic and non-hydrostatic pressures and τ_{xx}, τ_{xz}, τ_{zz}, τ_{zx} are the turbulent stresses (both normalized by the density).

The numerical method in SWASH model is based on an explicit, second-order accurate finite difference scheme where the mass and momentum are strictly conserved at the discrete level. The SWASH model uses sigma coordinates. A full description of the numerical model, BCs, numerical scheme and applications are given in [46].

3 Relaxation Zone (RZ) method

Relaxation zone (RZ) methods are typically implemented in mesh-based models (e.g. [47]) for wave generation/absorption. Only recently, [30] extended this methodologies to SPH. The method presented in [30] lays the groundwork for the implementation of a more generic wave generation and absorption method in DualSPHysics model. We refer here to implementation in 2DV or quasi-3D, which corresponds to the generation of long-crested waves in experimental wave facilities. A generation zone is arranged within the computational domain and particle velocities in the generation zone are forced to follow the orbital velocities of target waves. In [30] the particle velocity is controlled by analytical solution with a weighting C function, the shape of which resembles a cubic spline. The use of a weighting function prevents potential particle disorder due to the discontinuity of particle velocities at the interface between the RZ and main computational region. The velocities in the RZ are expressed as follows:

$$u_i = Cu_{ci} + (1-C)u_{pi} \tag{8}$$

$$w_i = Cw_{ci} + (1-C)w_{pi} \tag{9}$$

where u_i and w_i are the controlled horizontal and vertical velocities, u_{ci} and w_{ci} are the horizontal and vertical velocities calculated from the wave theory, u_{pi} and w_{pi} are the actual horizontal and vertical velocities calculated in the numerical model. DualSPHysics leaves the option to the user to use either the horizontal velocity only or both horizontal and vertical velocities to correct the particle kinematics. For all cases described in this paper, only the horizontal velocity has been used, namely Eq. (8), having verified that the differences with cases that use both velocity corrections are negligible. A damping area (i.e. passive absorption, see [16]) is introduced behind the RZ to eliminate unnecessary reflected waves from the rear side. It was finally verified that the spatial continuity of the pressure/density and velocity field is guaranteed at the interface between the RZ and the main fluid domain. Further evidence of it can be found in [48], where the continuity of both density and velocity field is shown for a case study of wave generation and wave impact on coastal defenses. The details are omitted here for sake of simplicity.

3.1 Weighting C function

Since the performance of the wave generation and reflection absorption can be decided by the shape of the C function, an arbitrary weighting function is introduced in the form of a hyperbolic function. For a specific width of the relaxation zone, W_{RZ}, the C function can be expressed as follows:

$$C(x,\psi,\beta) = \frac{\left\{tanh\left(\left(\frac{2x}{W_{RZ}}+\psi\right)\beta\right)-tanh\left(\left(\frac{2x}{W_{RZ}}-\psi\right)\beta\right)\right\}-\{tanh((1+\psi)\beta)-tanh((1-\psi)\beta)\}}{\{tanh(\psi\beta)-tanh(-\psi\beta)\}-\{tanh((1+\psi)\beta)-tanh((1-\psi)\beta)\}}, with\ -1 \le \frac{2x}{W_{RZ}} \le 1 \qquad (10)$$

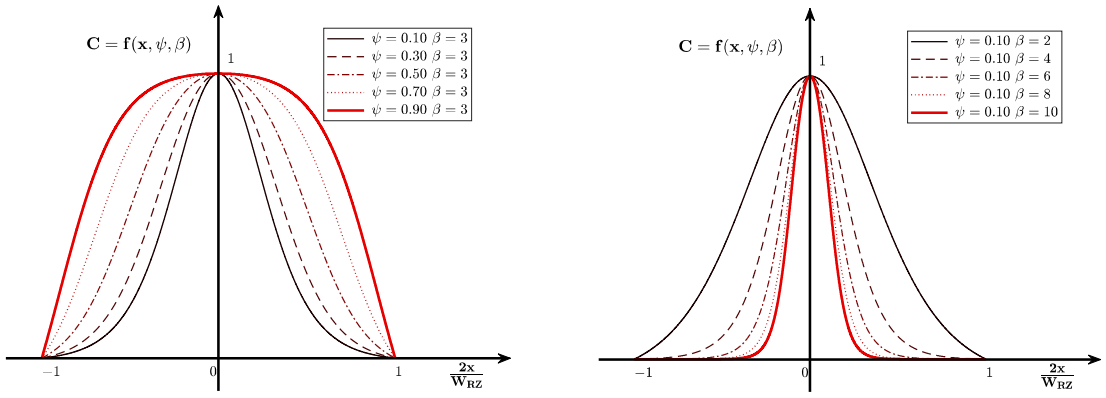

Figure 1. Shape of the weighting function C for different values of ψ and β

The value assumed by the function depends on the set of values chosen for the ψ and β parameters and on the distance from the center of the RZ, being zero at both extremes. The variation of the two parameters allowed exploring the performance of the RZ depending on the shape of C, as discussed in Section 4.2 of the present work. By changing ψ and β in the equation, the shape of the C function can be modified. Figure 1 shows some examples of the newly developed C function curve. The shape with ψ=0.3 and β=3 is quite similar to the one proposed by [30].

3.2 Effective width (W_{eff})

The performance of the relaxation zone technique to generate waves and to compensate wave reflection is related to effective width of the RZ. To take into account the effect that the C function exerts on it, it is possible to use a method to understand which part of the generation domain is responsible for generation behavior. The effective width of the RZ (W_{eff}), which is the area that rules the generation skill, is here introduced:

$$W_{eff} = (x_2 - x_1)W_{RZ}\ [m] \qquad (11)$$

where

$$x_1 \parallel C(x,\psi,\beta) = threshold \cup \frac{2x}{W_{RZ}} \ni [-1,0]$$

$$x_2 \parallel C(x,\psi,\beta) = threshold \cup \frac{2x}{W_{RZ}} \ni [0,1]$$

The scheme for the RZ and indication of the effective width are depicted in Figure 2. The area bounded by the red dashed line corresponds to the RZ. The waves generated within the RZ will propagate in both directions along the x-axis. At the right side of the RZ there is the main fluid domain where the waves will freely propagate. At the left-side of the RZ, bounded by a blue dashed line, it's the damping area, where the waves that are propagating behind the RZ will be absorbed. This extra fluid area is necessary to guarantee continuity in the fluid domain inside the RZ.

It is assumed that not the entire RZ zone contributes in the same way to the wave generation, but only the part of it where the tails of the C function might have negligible contribution. This has been verified trying to correlate the accuracy (i.e. error) in wave generation with the size of the generation zone and the dimensionless wave length (W_{RZ}/L); however, the correlation was very poor. When a threshold is defined in order to consider only W_{eff} instead of W_{RZ}, the correlation between the error and the RZ domain increases. See Section 4.2 for detailed error analysis.

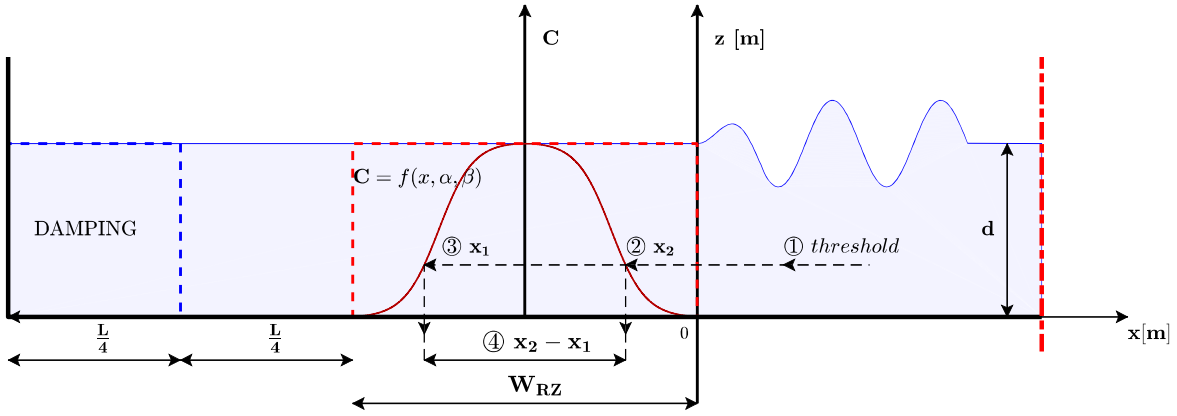

Figure 2. Scheme of RZ (red dashed line) and indication of the effective width in case of wave generation. The damping area behind the generation zone is indicated by a dashed blue line. A threshold for the *C* function is defined (1) and determines the values assumed by the function (2,3) which define the effective width of the relaxation zone (4)

For wave reflection it is expected that the tails of the RZ might affect the compensation of the reflected waves, being that the first part of the RZ that is encountered by the waves when they are travelling back. For this reason the definition of the effective width for wave reflection, $W_{eff.R}$, has been modified as follows (see Figure 3):

$$W_{eff.R} = \frac{x \cdot W_{RZ}}{2} \ [m] \tag{12}$$

where

$$x = (1 - |x_1|) \ for \ x_1 \parallel C(x, \psi, \beta) = threshold$$

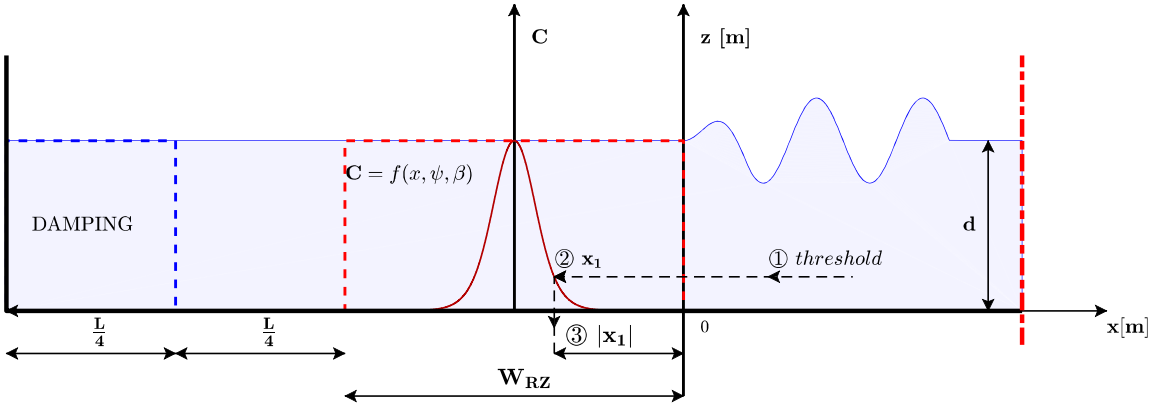

Figure 3. Scheme of RZ (red dashed line) and indication of the effective width in case of wave reflection. The dashed blue line indicates the damping behind the RZ. A threshold for the *C* function is defined (1) and determines the value assumed by the function (2) which defines the width of the RZ tail affecting wave reflection compensation (3)

3.3 RZ for model coupling

One of the interests concerning practical applications in coastal engineering is how the RZ method works for coupling DualSPHysics to wave propagation models, particularly to SWASH, for which a different hybridization technique was already implemented in [14]. As described earlier, the particle velocity in the RZ is controlled by the analytical solution with a weighting function C. However, for the coupling, SWASH output can be used in the RZ, instead of the analytical solution. Eq. (8) and Eq.(9) are used to express the velocities in the relaxation with the only difference that the values of the horizontal and vertical velocities calculated from the wave theory, u_{ci} and w_{ci}, are replaced by u_{si} and w_{si}, which are the horizontal and vertical velocities calculated in SWASH.

With reference to the coupling, SWASH is employed using a multi-layer approach: the time series of the velocity per each SWASH layer is used. Performing a multi-layer calculation, the velocity of the SPH fluid particles in the RZ is calculated by a smooth interpolation of the average velocity of each layer in SWASH, where the velocity is considered uniform in each layer at a certain time. During the interpolation procedure, the velocity is considered applied to the center of each layer. The velocity of the lowest layer (i.e. closest to the sea bottom) is extended uniformly up to the bottom. For the particles on the free-surface, the velocity is assumed the same as the average velocity of the uppermost layer in SWASH simulation. It has to be noticed that the vertical dimension of each layer varies in time depending on the instantaneous water surface elevation. This means that the vertical coordinate of the center of each layer (where the velocity is assumed as applied) varies in time. This variation is taken into account for the interpolation procedure. The optimal number of layers in SWASH has been investigated in [14]. Similar investigation has been carried out in the present work, showing that there is an increase in the model accuracy up to 8 layers, after which the improvement is negligible. Therefore, an 8-layer calculation has been performed for all cases presented in the next sections. To reconstruct the velocity profile in the RZ, several measurements along the direction of wave propagation are need in SWASH to cover the whole generation area. After several trials, a number varying between 20 and 40 measurement sections in SWASH covering the whole RZ yielded an accurate velocity profile. After vertical interpolation for each of these positions, a horizontal interpolation is performed as well, hence the whole RZ is covered and orbital velocity values (u_{si} and w_{si}) are applied to all SPH fluid particles in the RZ. Finally, interpolation in time is needed as well, because of the calculation time step in DualSPHysics being smaller than the corresponding one in SWASH.

3.4 Drift correction

Non-linear effects cause a drift in the particle displacement far from the generation zone. This drift is actually the mass transport predicted by Stokes at 2nd order solution for monochromatic waves. The particles experience a drift velocity that can be expressed by

$$\overline{U}(z) = \frac{\xi(\tilde{x},\mathrm{z},\mathrm{T}) - \xi(\tilde{x},z,0)}{T} = \left(\frac{\pi H}{L}\right)^2 \frac{C}{2} \frac{\cosh\left[\frac{4\pi(z+d)}{L}\right]}{sin^{\,2}\left(\frac{2\pi d}{L}\right)} \tag{13}$$

This fact leads the water level in the fluid domain to increase, because particles are pushed out of the generation zone. The water level in the generation zone consequently decreases. The increase water level in the main numerical domain, outside the generation zone, has been estimated in terms of volume variation. An example of the cumulative volume increase in time is reported in Figure 4 (drift=OFF), together with the predicted one, if Eq. (13) is used. One can see that measured volume increase matches the predicted one. This confirms that above assumption.

To avoid unrealistic increase of water level outside the generation zone, a correction to prevent this drift has been implemented. This correction is proportional to the velocity as predicted by Stokes'. For the case of irregular waves, the correction is calculated and applied for each single wave that forms the wave train. The wave height and period used for the correction calculation are calculated using zero-down crossing method. Results using the correction treatment for the drift are depicted in Figure 4 (drift=ON). If, without correction, the increase in volume in the main fluid domain was about 3.5% for this specific

example, the volume increase with correction is almost zero. This has been verified for several cases, with different wave conditions and fluid domain sizes.

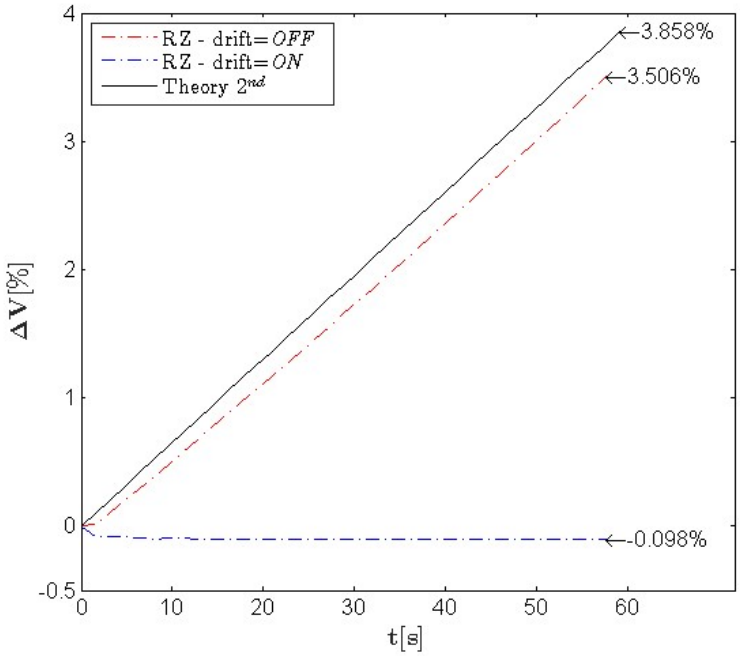

Figure 4. Cumulated volume related to the total one due to drift: with no correction (red) and with correction treatment (blue).

4 Applicability of RZ for wave generation and reflection compensation for regular waves

Applicability of RZ to a highly reflective condition is investigated here as one of the benchmark tests. The highly reflective condition is practically the most critical case for the reflection absorption. Therefore, once a model is validated for wave generation and reflection absorption under such a condition, it guarantees that the model works properly in most of the coastal engineering applications.

4.1 Model setting

4.1.1 Calculation domain and applied waves

The performance of RZ method is tested for regular waves. The reason of using regular waves is that it is straightforward to recognize even small influences on the free surface caused by possible inaccuracies in generation and absorption. Figure 5 shows the model setup for the sensitivity analysis of wave generation (with damping area at both sides of the domain) and applicability test under highly reflective conditions (without damping area at the right-hand side). For the applicability tests, 20 wave gauges were placed close to the right-hand side wall equally distributed over a length of $L/2$. These measurement points have been used to reconstruct the reflection pattern (i.e. standing wave) in front of the vertical wall.

Ten different wave conditions have been tested. The values of wave height H, wave period T and water depth d are reported in Table 1 together with the wavelength L and wave steepness. The wave conditions have been chosen in order to cover a wide range of wave steepness, from 1.08% (low steepness) to 3.52% (high steepness). Note that the wave conditions are limited to the regime of Stokes 2nd order theory (Figure 6).

The initial interparticle distance for each simulation has been selected accordingly to [16], in particular H/dp = [8, 12]. A sensitivity analysis on the model resolution has been conducted. It will be shown later on in this work, for the cases of random waves.

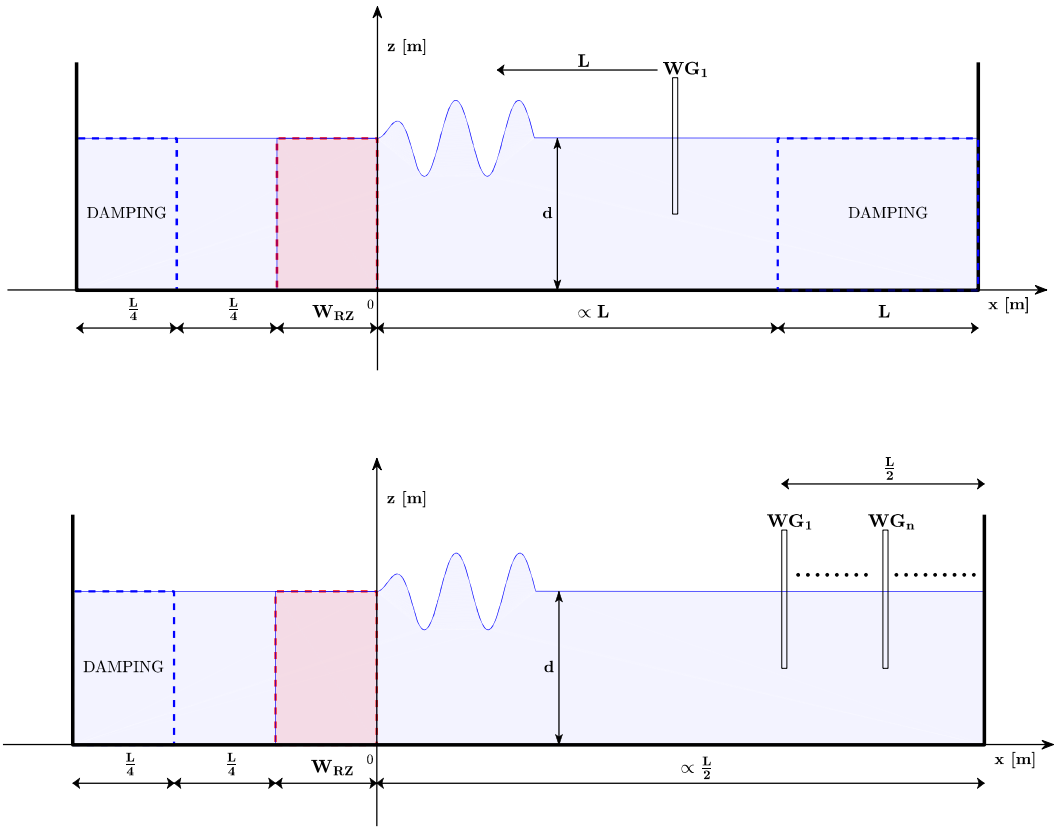

Figure 5: Model set-up of the sensitivity analysis for wave generation (upper panel) and applicability test under the highly reflective condition (lower panel). RZ (red area), damping areas (blue dashed lines). WG_1-WG_n indicate the wave gauges for reflection analysis in the highly reflective case.

Table 1: Wave conditions applied to the benchmark test

Case	Wave height [m]	Wave period [s]	Water depth [m]	Wave length [m]	Wave steepness [%]
1	0.100	1.60	0.80	3.55	2.82
2	0.125	1.60	0.80	3.55	3.52
3	0.075	1.60	0.80	3.55	2.11
4	0.100	1.80	0.80	4.22	2.38
5	0.100	1.40	0.80	2.88	3.47
6	0.100	1.60	1.00	3.73	2.68
7	0.100	1.60	0.60	3.27	3.06
8	0.040	2.00	0.40	3.69	1.08
9	0.100	3.00	1.00	8.69	1.15
10	0.030	1.70	0.30	2.71	1.11

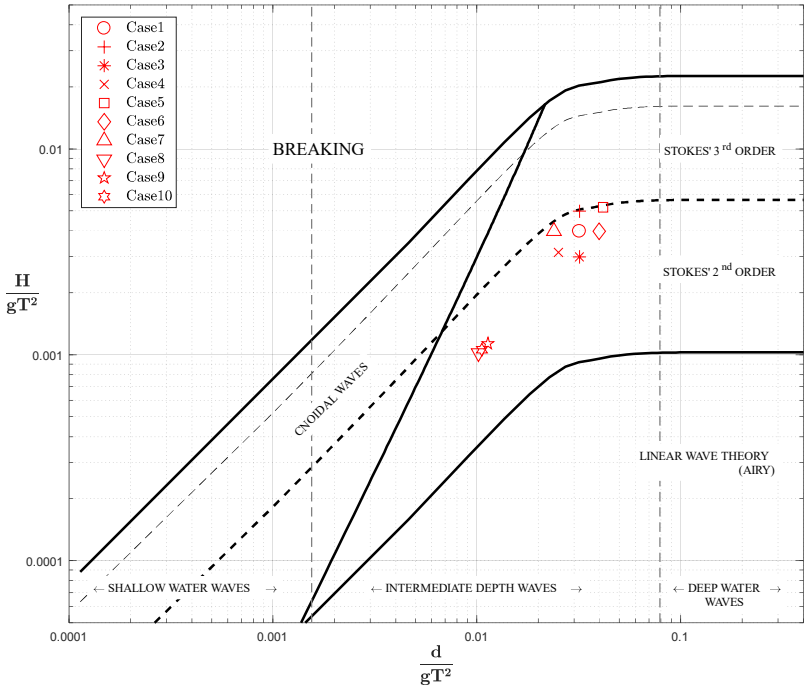

Figure 6: Tested wave conditions plotted in Le Mèhautè diagram for wave generation and applicability test under the highly reflective condition.

4.1.2 Method for wave reflection analysis

For the highly reflective cases (i.e. vertical wall without sponge layer at the right-hand side of the domain), reflected waves and re-reflected waves are analysed to investigate the performance of RZ. Note that the 'reflected waves' means the waves reflected one time at the vertical wall, and 're-reflected waves' includes reflection (if applicable) at the generation zone. The time window, Δt, between each reflection and re-reflection event has been identified, characterised by the initial time t_1, t_2…, t_i (see Figure 7).

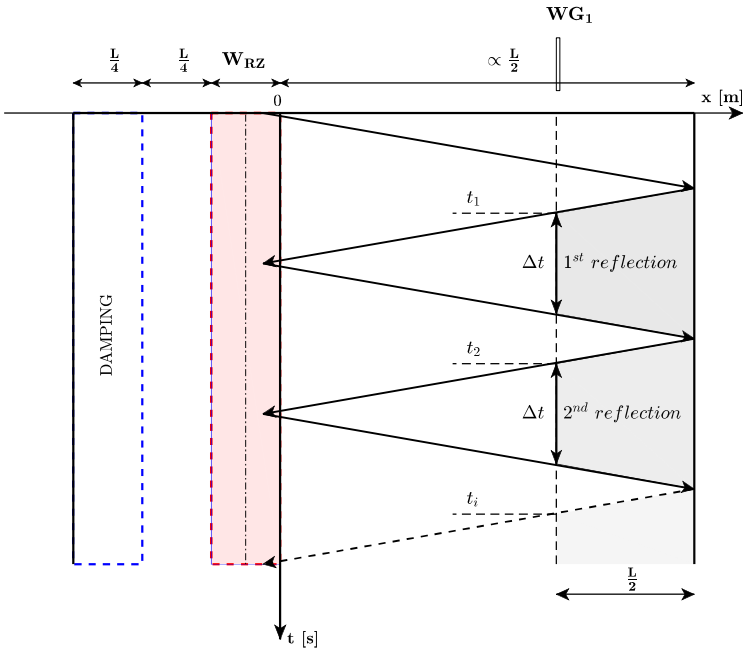

Figure 7: Time window for reflected waves and re-reflected waves. Δt indicates the time between each reflection and re-reflection event.

4.2 Model applicability using arbitrary *C* function

4.2.1 Wave generation

Before analysing highly reflective cases, the accuracy of RZ in only wave generation mode has been assessed. Initially a combination of ψ and β equal to 0.35 and 5 respectively with $W_{RZ}=L$ has been used for wave generation. The dimension of the main numerical domain outside the RZ zone is equal to 2L. For all cases the free-surface elevation was accurately modelled, independently of the wave height and wavelength. Results can be seen in Figure 8, where the free-surface elevation and orbital velocities are plotted for test cases 1-5. The horizontal and vertical orbital velocities have been measured at x=*L* and z=*d/2*, where d is the water depth. The free-surface elevation has been measured at x= *L*. The results demonstrate that RZ is able to generate the target waves accurately. Cases 6-10 present the same level of accuracy of those shown in Figure 8 and therefore are omitted for sake of simplicity.

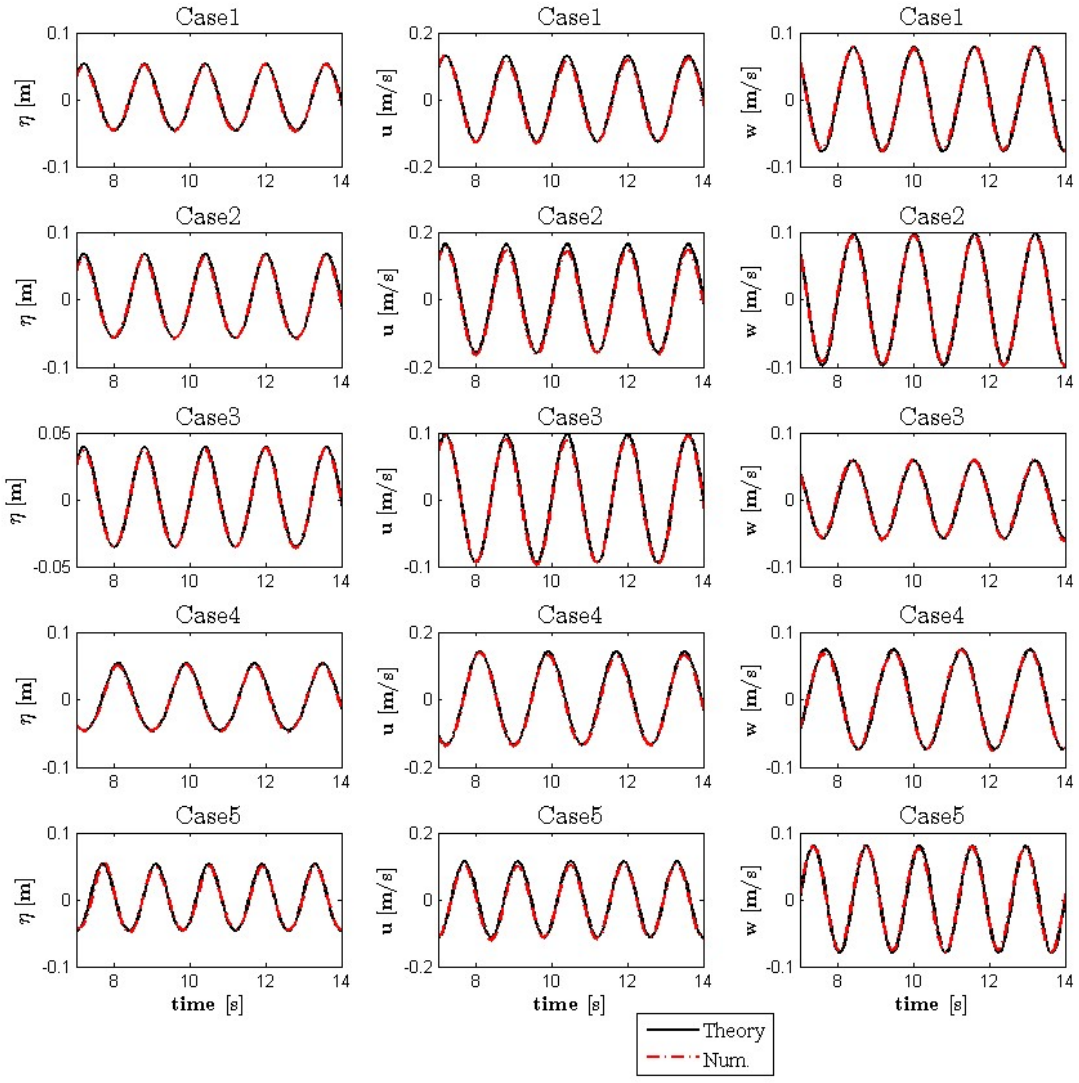

Figure 8. Water surface elevation measured at x=L and orbital velocities measured at x=L and z=d/2 for test cases 1 to 5.

In Section 3.2, the effective width of the RZ has been introduced (W_{eff}), stating that the performance of the RZ to generate waves and to compensate wave reflection might be related to W_{eff}. All ten cases have been simulated varying W_{RZ} (between L/12 and L), ψ (0.1-0.7) and β (5, 7, 9), obtaining 900 numerical simulations. For each simulation the accuracy has been estimated using the following error parameter:

$$\epsilon = \left(mean\frac{|H_{SPH}-H_{Th}|}{H_{Th}}\right)\cdot 100\ [\%] \tag{14}$$

where H_{SPH} is the numerical wave height and H_{th} is the target theoretical wave height. The error parameter is related to the effective dimension of the RZ as expressed by Eq. (11), in which the threshold value has been assumed as C=0.15, after having explored different values between 0 (=whole C function, $W_{RZ}=W_{eff}$) and 0.9. The variation of ε with the non-dimensional quantity W_{eff}/L is depicted in Figure 9. The figure shows that the error decreases up to a value of W_{eff}/L equal to 8 %, after which the numerical model predicts the waves with a difference of only 2-3%. It is important to notice that the accuracy of the RZ increases as the wave steepness decreases: for Cases 8-10, the error is actually independent on the size of the RZ zone. Related to the smoothing length, the error is less than 10% of h_{SPH} when W_{eff}/L is equal or larger than 8 %. The choice of ψ and β for wave generation determines the shape of the weighting function C and, therefore, the ratio between value of W_{eff} and W_{RZ} once the threshold is fixed. For any combination of ψ and β, Figure 9 shows that it is finally the effective dimension of RZ related to the wave length that plays the major role. In the following section the procedure to set the source generation zone and the C function is described.

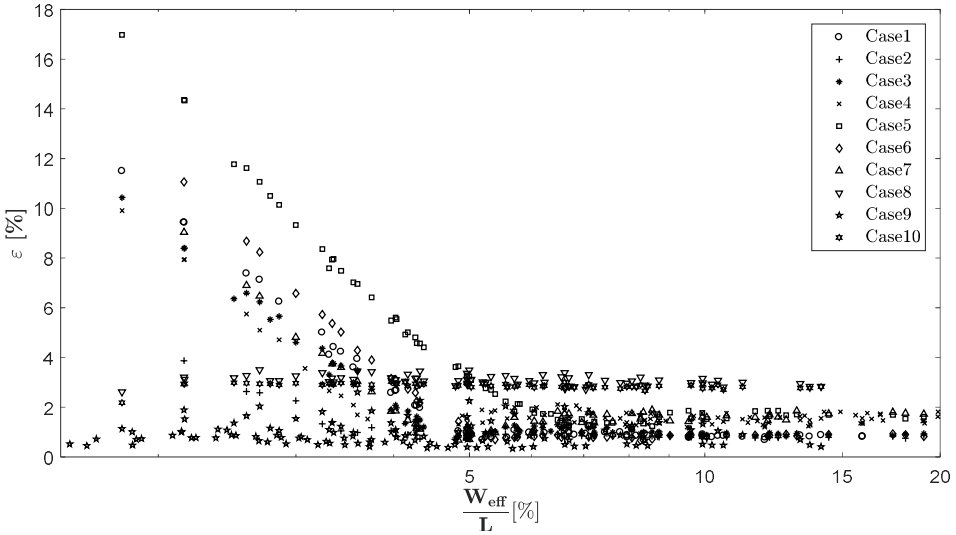

Figure 9. Error in wave height measured at x=L as function of the effective size of the RZ zone.

4.2.2 Design of RZ for wave generation

In this section the procedure for RZ setup in DualSPHysics for wave generation of regular waves is explained based on the results above discussed. A threshold C=0.15 has been used and, based on Figure 9, it is assumed that for $W_{eff}/L \geq 0.08$ the numerical error is below 3%. Therefore, an abacus has been reconstructed (see Figure 10): each isoline in the abacus corresponds to a different ratio between the effective size of the RZ and the RZ dimension, $k_{eff}=W_{eff}/W_{RZ}$. Then, the procedure for the RZ design can be summarized as follows:

1. Calculate L, wavelength, based on wave period and water depth.
2. Determine the effective size of the RZ, as $W_{eff} \geq 0.08 \cdot L$
3. Select the isoline in the abacus ($k_{eff} \in [0.80,0.90]$ is suggested)
4. Then, calculate $W_{RZ} = W_{eff}/k_{eff}$
5. According to your choice of k_{eff}, fix the value of ψ (or β) to determine from the abacus the right value of β (or ψ).

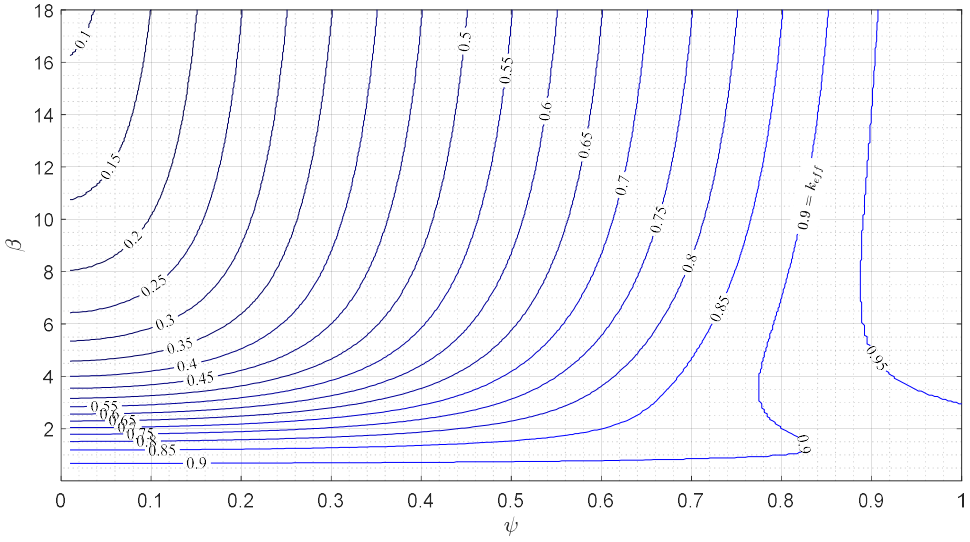

Figure 10. Abacus for design W_{RZ} parameters for a value of threshold $C=0.15$

For random waves, the wavelength L can be replaced by L_p, being the wavelength calculated employing the peak period T_p. However it is recommended to use wider RZ for random than for regular waves, in order to consider lower frequency components of the wave spectra.

4.2.3 Wave reflection

The compensation of reflected wave energy is a key aspect of wave generation, for physical models and numerical models. Without a proper and efficient reflection compensation there will be an undesirable increase of wave energy in the numerical/experimental domain that will bias the results of the model. To prevent the re-reflection of the waves that, after a first reflection at the coastal structure, reach the generation system, an absorption technique must be implemented. In DualSPHysics this has been done implementing an Active Wave Absorption System (AWAS) when moving boundaries are used to generate waves. For RZ, in principle, there is no need of implementing any absorption technique since every time step the orbital velocity is imposed to the fluid particles in the RZ zone, as expressed by Eqs. (8) and (9). Nevertheless, the accuracy of RZ to absorb reflected wave needs to be demonstrated. To do that, the same cases as in Table 1 have been simulated, but removing the damping at the right-hand side of the domain. In this way, the waves are reflected back towards to the RZ zone by the boundary particles forming the vertical wall that limits the fluid domain, as depicted in Figure 5. Case 1 has been selected for a detailed analysis on wave reflection compensation. Initially, the dimension of the main numerical domain and W_{RZ} have been set equal to L. Different shapes of the weighing function C have been analyzed, resulting the best value of β equal to 5 and the best values for ψ ranging between 0.23 and 0.32. In case of vertical wall, total reflection is expected with the formation of standing waves with nodes and antinodes. The free-surface elevation at the antinode ($x=L$) is plotted in Figure 11 and compared with the theoretical one for waves belonging to 2nd order Stokes' theory. At long term, the RZ compensates the wave reflection efficiently: the time series of numerical free-surface elevation matches the theoretical one. However, a transitional phase is present at the beginning of the time series, when the RZ seems to react to the reflected waves. The duration of this phase is equal to about 10 wave periods in case of main domain size equal to L, however it has been verified that increasing the domain size, the duration of the transitional phase decreases, because it depends directly on the time that the waves need to propagate after each reflection. The water surface elevation at the node ($x=3/4L$) is not plotted but it was verified that it matches the expected one, with the amplitudes at node very small as predicted by the second-order solution.

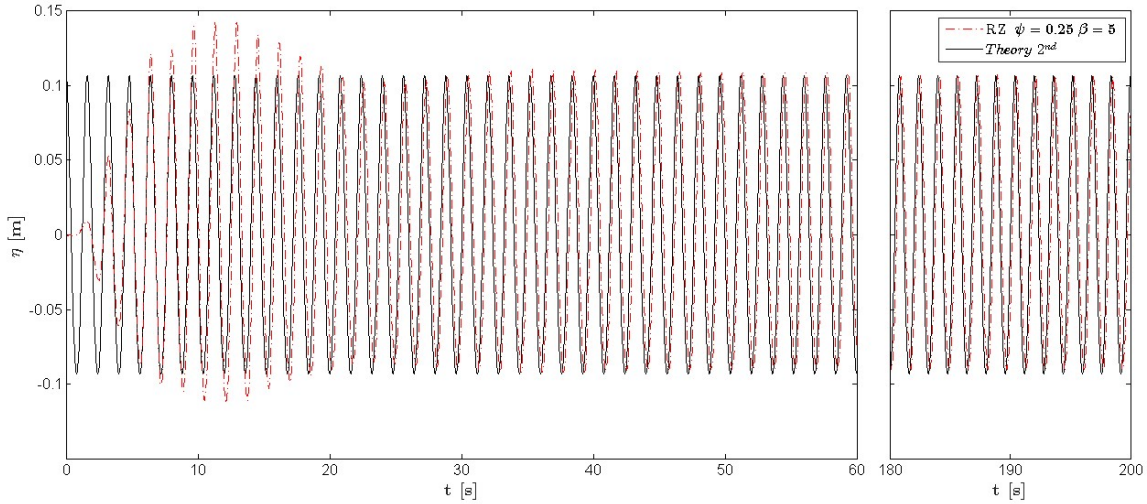

Figure 11. Wave profile at antinode (x=L) for Case 1 with highly reflective conditions

The numerical error has been quantified as follows:

$$\overline{\epsilon_R} = \frac{\sum_{i=n_{tr}}^{end}\left(\epsilon_{R,t_i+\Delta t}\right)}{end-n_{tr}} \tag{15}$$

with

$$\epsilon_{R,t_i+\Delta t} = \left(\frac{H_{SPH,t_i+\Delta t}-2CR\cdot H_{Th}}{2CR\cdot H_{Th}}\right)\cdot 100\ [\%] \tag{16}$$

where n_{tr} is the number of cycles (each cycle=Δt in Figure 7) excluded because of the transitional phase shown as example in Figure 11; t_i is the initial time of each *i-th* reflection time window; Δt, as represented in Figure 7, $H_{SPH,t+\Delta t}$ is the wave height averaged over each Δt at the antinode location; $2CR\cdot H_{th}$ is the theoretical wave height at antinode, where CR is the theoretical reflection coefficient, equal to 1 in case of full reflection. The results of ε_R for each Δt are depicted in Figure 12: after the first transitional phase, the numerical error is small, namely between -5% and 8%, being this range still smaller than the smoothing length value.

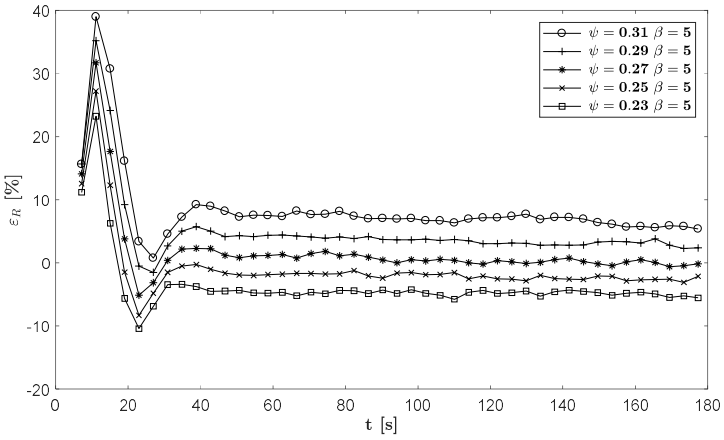

Figure 12. Accuracy of wave reflection (Case 1)

4.2.4 Design of RZ for wave reflection

In this section the procedure for RZ setup in DualSPHysics for wave reflection of regular waves is explained for highly reflected cases (e.g. vertical walls, steep dikes, non-overtopped structures). In Section 3.2, the effective width of the RZ for wave reflection has been introduced ($W_{eff.R}$). To evaluate the performance of the RZ in case of highly reflected cases, all ten cases in Table 1 have been simulated varying W_{RZ} (L/2 and L), ψ (0.05-0.5) and β (2-9) and the physical time per simulation has been set equal to 150 s, obtaining 1200 numerical simulations. After several trials, a threshold C=0.0005 has been selected.

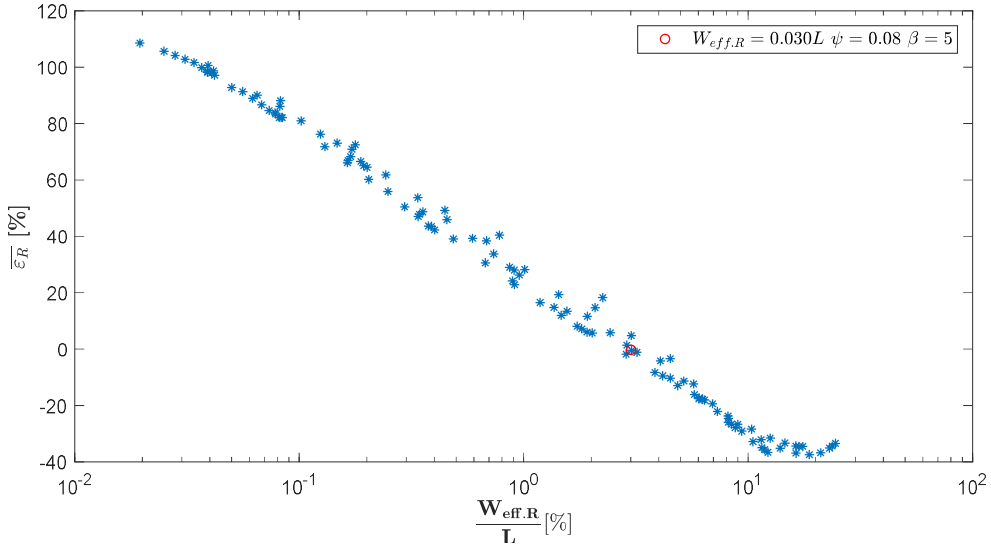

Figure 13. Error in reflected wave height as function of the effective size of the RZ zone for highly reflective cases (Case 1). The primal set of parameters is marked with a red dot.

Figure 13 shows the numerical error in the reflected wave height as function of the effective size of the RZ zone for Case 1. The optimal set of parameter is marked with a red dot and corresponds to ψ=0.08, β=5 and $W_{eff.R}$≈0.030L. Similar values are obtained for the other test cases.

A linear relationship between the ratio $W_{eff.R}/L$ and the wave energy flux has been noticed (Figure 14). The wave energy flux for each test case has been calculated as follows:

$$\overline{e} = \frac{\overline{E}}{d} = \frac{1}{d}\frac{E}{L}\ [\frac{J}{m \cdot m}] \tag{17}$$

where E is the total wave energy (=$\rho g H^2 L/8$), L the wavelength, d the water depth and H the incident wave height.

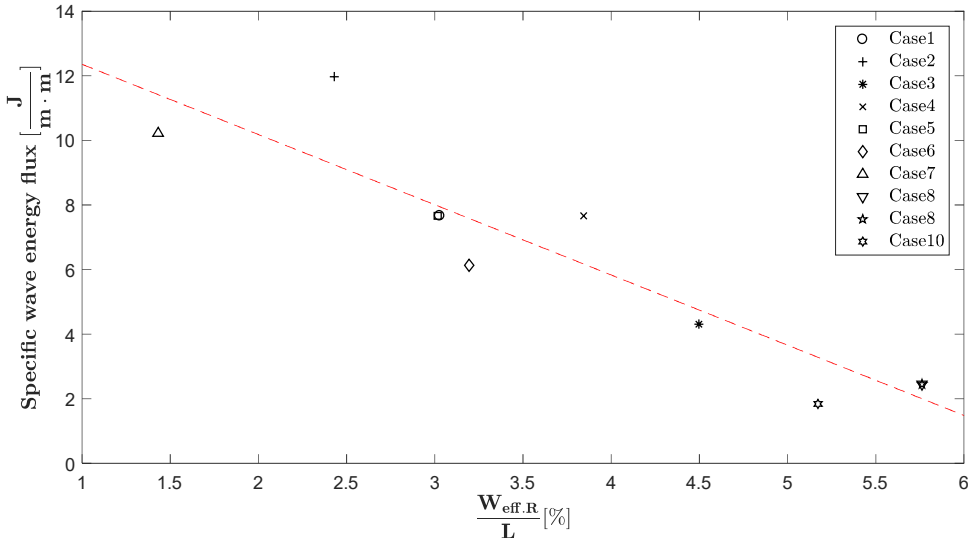

Figure 14. Relationship between wave energy flux and the effective width of the RZ for wave reflection. Linear regression is applied to the data (dashed line).

Once is known the wave specific energy flux, one can select the value of $W_{eff.R}$ from Figure 14 and the size of the RZ, W_{RZ}, can be calculated as follows:

$$W_{RZ} = \frac{W_{eff.R}}{1-|x_1|} \tag{18}$$

where x_1 is calculated in order to get $C(x_1, \psi, \beta) = 0.0005$. In general, it has been verified that a combination of values of ψ and β relatively small, namely $\psi \leq 0.4$ and $\beta \leq 5$, makes the velocity correction as expressed in Eq. (8) and Eq. (9) smooth, allowing particles to vary slowly their own velocity to approximate the theoretical one once they are close to the center of the RZ zone.

4.3 Model applicability using RZ to couple DualSPHysics and SWASH

4.3.1 SWASH model setting

Numerical simulations were carried out with SWASH. The numerical test layouts described were reproduced in the SWASH numerical domain. The grid size in the x-direction was set as 0.02 m for all cases. The model was run with 8 layers in the vertical direction. The incident wave time series was prescribed at the wave boundary in the numerical model simulations with a weakly reflective boundary condition. A Sommerfeld radiation condition and a sponge layer was applied at the end of the numerical flume in order to minimize the effect of the reflection. The numerical time step is automatically changed during SWASH calculations to satisfy the Courant–Friedrichs–Lewy (CFL) condition. No bottom friction was used in all numerical simulations. The non-hydrostatic pressure term was applied with the classical central differencing scheme. Explicit time integration was used with a time step restriction set to a maximum Courant number of 0.5.

4.3.2 Wave generation

Test Case 1 has been selected for RZ applied for coupling DualSPHysics to SWASH. Same case setup and characteristics as of RZ only have been used. The only difference is that the target orbital velocities are extrapolated by SWASH instead of being calculated using the 2nd order Stokes' wave theory. An example of the DualSPHysics free-surface elevation is depicted in Figure 15, together with SWASH solution. The case refers to $W_{RZ}=L/2$, $\psi = 0.50$ and $\beta = 6$, with size of main numerical domain equal to 2L. The numerical error, calculated using Eq. (14) is plotted in Figure 16 as function of W_{eff}/L, for 180 different combinations of ψ and β and W_{RZ}. The model accuracy varies accordingly to Figure 9: for $W_{eff}/L > 0.08$ the error is about 2-4%. Thus, same procedure to setup the RZ zone as described in Section 4.2.2 can be

used. It is worthy to notice that it is recommended to apply only 10% of the drift correction when SWASH velocities are used as input for the RZ, because the velocity field in SWASH differs from the theoretical one prescribed by Eq. (14) which does not predict the undertow.

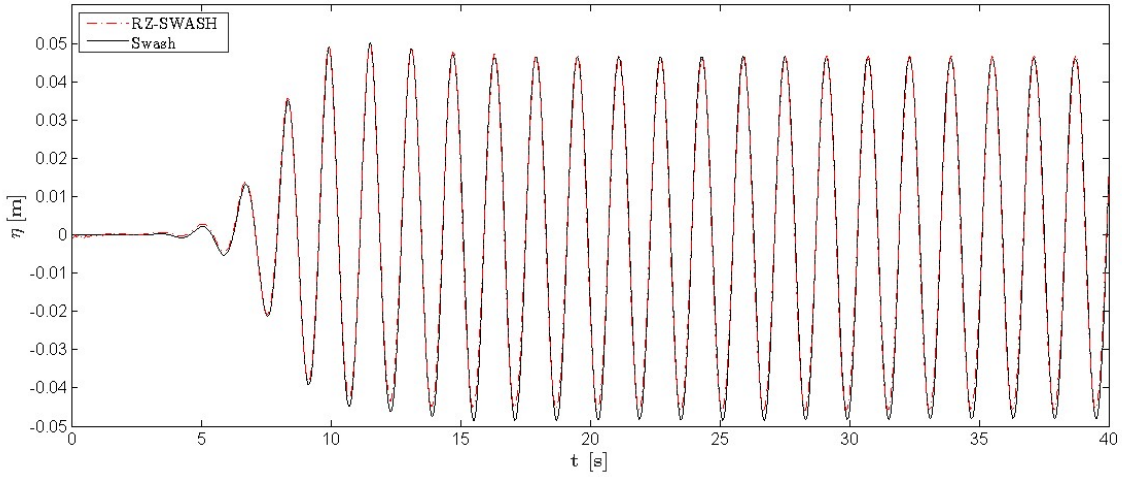

Figure 15. Wave profile at $x=L$ (Case 1) for RZ applied for coupling between DualSPHysics and SWASH

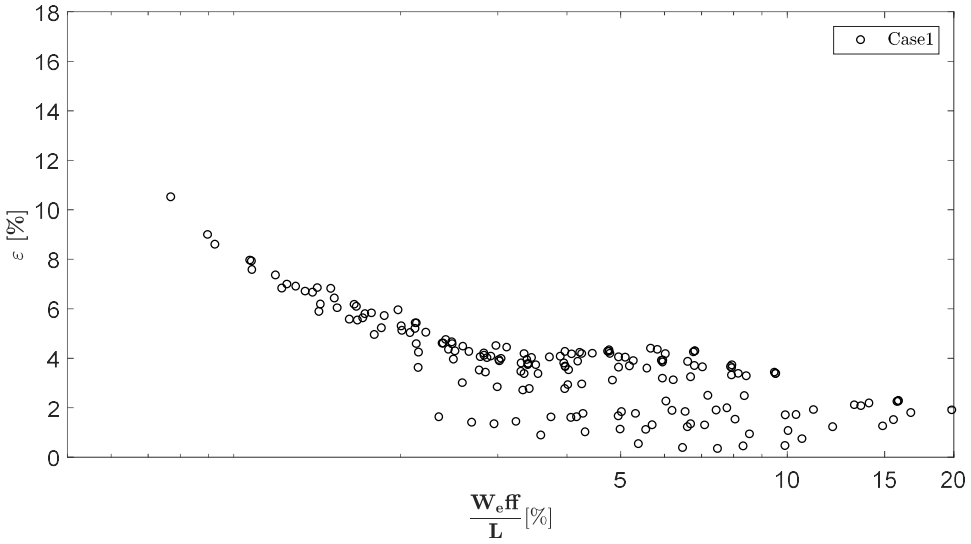

Figure 16. Wave height error at $x=L$ (Case 1) for RZ applied for coupling between DualSPHysics and SWASH

4.3.3 Wave reflection

Wave reflection compensation for RZ applied to couple DualSPHysics and SWASH has been tested for Case 1. Results of the time series at antinode are depicted in Figure 17. A transitional phase is present as in the case of RZ only. After this phase, the model responds efficiently to absorb the reflected waves and the error varies between -10% and 1% approximately depending on the values used for ψ and β with similar behaviour to the one shown in Figure 12. At the node the oscillation of the water surface is practically zero, as expected.

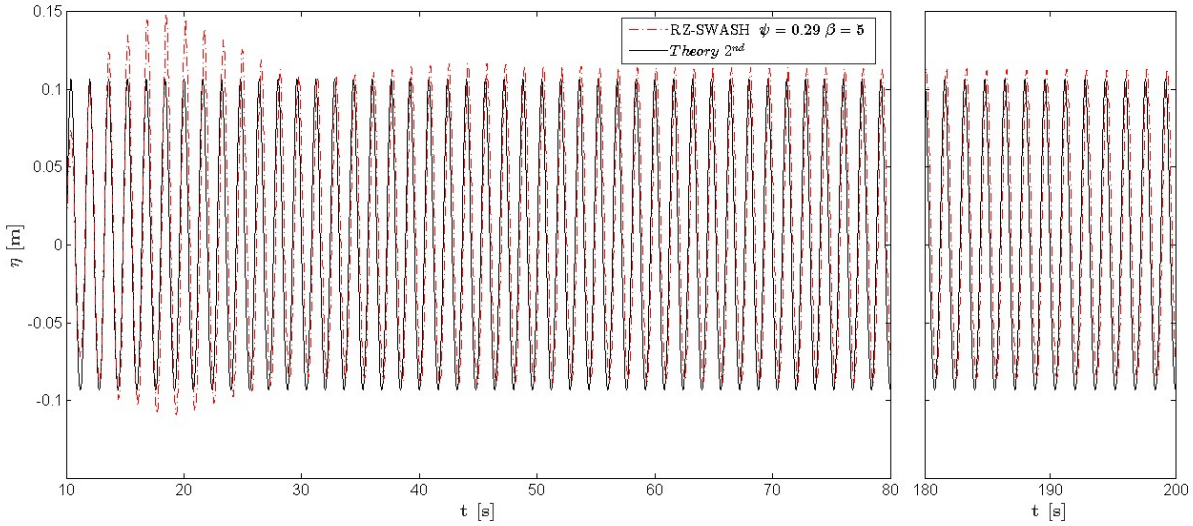

Figure 17. Wave profile at antinode (x=L) for RZ applied in the case of coupling between DualSPHysics and SWASH in highly reflective conditions

5 Extension to irregular wave generation for real sea states

So far, the application and accuracy of RZ has been discussed for cases with regular waves only. Extension to irregular wave cases are discussed in the present section. A JONSWAP spectrum has been used to generate an irregular wave train with significant wave height H_{m0}=0.10 m, peak period T_p=1.60 s for a water depth d=0.80 m. A stretched algorithm as described in [16] is used to define the bandwidth. As for the parameters, it has been used the following set W_{RZ}=L_p, $\psi = 0.50$ and $\beta = 6$ and drift correction value equal to 1.05. A total duration of 500 s has been simulated, corresponding roughly to 350 waves, using a TITAN X graphic card.

First, DualSPHysics as stand-alone model has been used. The waves are generated by means of the RZ technique. The numerical free-surface elevation is plotted in Figure 18 for the first 100 s of simulation, as measured at L_p from the RZ zone. The theoretical time series is also represented for comparison.

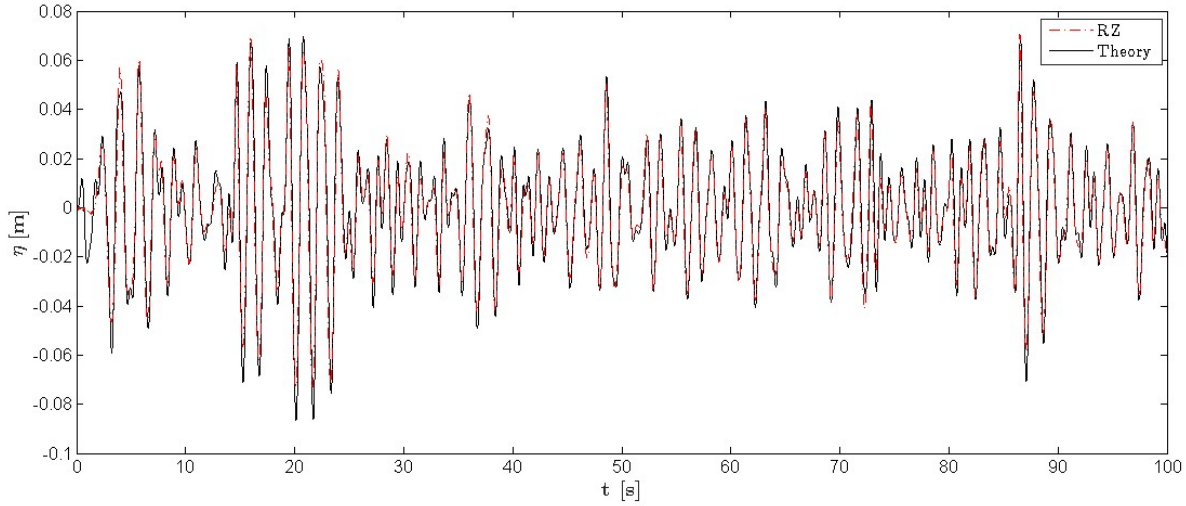

Figure 18. Free-surface elevation in case of irregular waves measured at x=L, comparison between RZ and target signal.

5.1.1 Convergence analysis

A sensitivity analysis on the initial interparticle distance, *dp*, has been performed. Five cases, using the previous parameter setting, have been simulated with *dp* equal to 1/6, 1/8, 1/10, 1/12 and 1/16 of the significant wave height H_{m0}. Spectral parameters such as the significant wave height, H_{m0} ($=4\sqrt{m_0}$) and the spectral period $T_{m-1,0}$ ($=m_{-1}/m_0$) have been calculated and compared with the ones derived from the theoretical time series. The results are reported in Table 2, together with the total number of fluid particles *Np* and the computational runtime. The wave spectra for all cases are depicted in Figure 19. All measures refer to $x=L_p$ (distance from RZ). In general, the target wave conditions are accurately predicted in the range of dp/H used for the present analysis, with an error on H_{m0} that varies between 4% and 5%. Lowest accuracy is attained for $dp=H_{m0}/6$. Due to the small differences between $dp=H_{m0}/8$ and $dp=H_{m0}/16$, a reasonable compromise between model accuracy and computational runtime has been found using $dp=H_{m0}/10$. The choice of this value is also corroborated by [16] and [44] .

Table 2. Sensitivity analysis: spectral parameters for different *dp* in comparison with the target wave conditions

SPH	dp/H_{m0} [-]	Np	Runtime [h]	H_{m0} [m]	T_p [s]	$T_{m-1,0}$ [s]
1	1/6	49914	3.4	0.0950	1.628	1.629
2	1/8	71568	5.5	0.0952	1.628	1.542
3	1/10	140225	11.9	0.0957	1.628	1.509
4	1/12	205344	19.2	0.0960	1.628	1.526
5	1/16	355068	40.7	0.0959	1.628	1.508
TARGET				0.1003	1.628	1.460

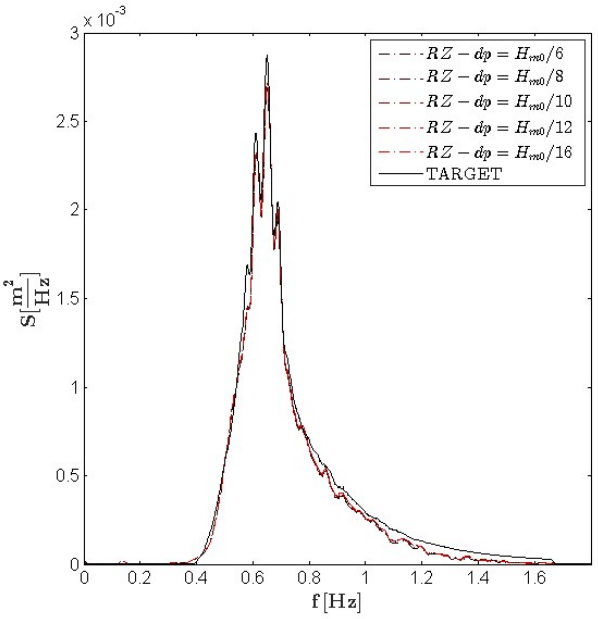

Figure 19. Sensitivity analysis: wave spectra in case of irregular waves, comparison between RZ results and theoretical spectrum.

An extra case has been simulated for $H_{m0}/dp=10$, where the piston-type wave generator [16] has been used instead of the RZ to generate the same irregular wave time series. The goal was to compare the accuracy of both generation systems as implemented in DualSPHysics. The wave spectra for the RZ and piston-type models are depicted in Figure 20 together with the one calculated on the target wave time series. The

calculate values of H_{m0}, T_p and $T_{m-1,0}$ are also plotted. Both generation techniques are demonstrated to be accurate. They actually give very similar results.

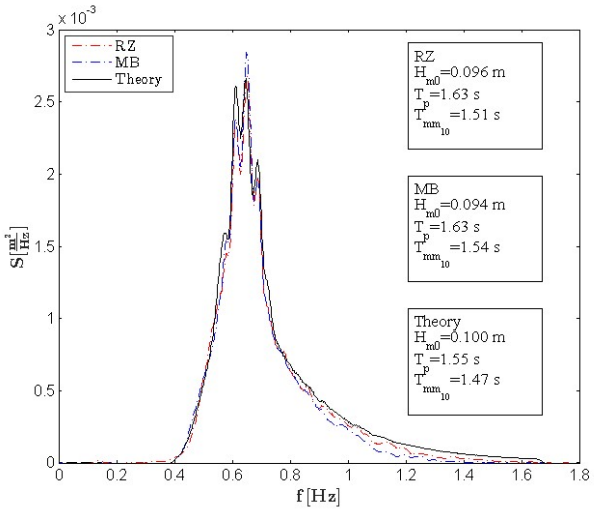

Figure 20. Wave spectra in case of irregular waves, comparison between RZ, piston-type generation (MB) and theoretical results for Case 1 and H_{m0}/dp=10.

When RZ is applied to couple DualSPHysics to SWASH model, the velocity data from SWASH are used as input for the relaxation zone. Notice that the resulting orbital velocities might be slightly different from those prescribed by theory, being the velocity in SWASH the average velocity per each layer used in the vertical discretization of the water depth. Then, the drift correction (equal to 0.50 in this specific case) has been applied. The water surface elevation measured at x=L in the SPH domain and the one acquired from SWASH simulation are plotted in Figure 21.

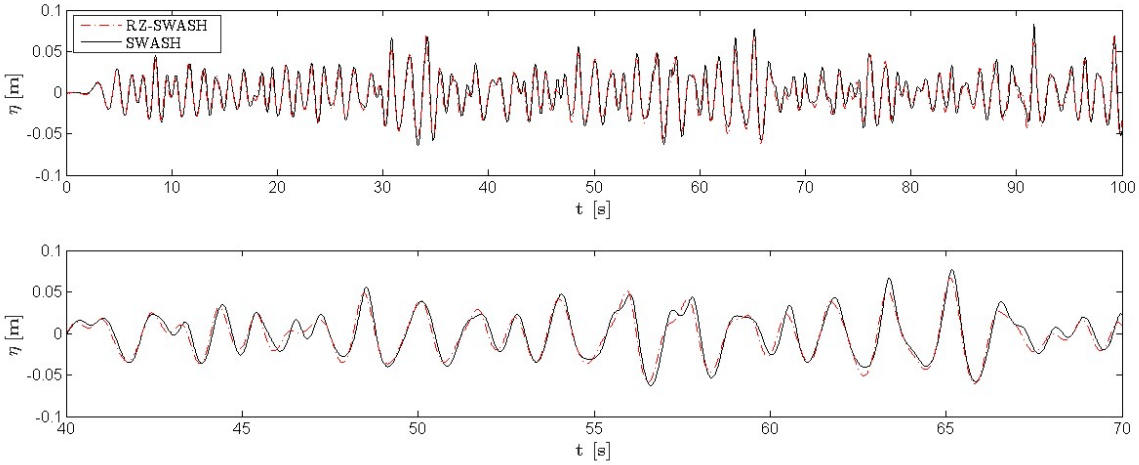

Figure 21. Free-surface elevation in case of irregular waves measured at x=L, comparison between RZ applied to model coupling and SWASH results.

Finally, a case in highly-reflective conditions has been modelled to assess the response of the RZ to reflected waves in case of random wave trains. The horizontal velocity field in SPH domain at t=244.4 s is plotted in Figure 22a together with five measurements points (black dots) where the water surface elevation has been measured. The location of these numerical wave gauges was x=[4.43 m, 4.61 m, 4.86 m, 5.18 m, 5.53 m]. The same case, but with damping area at the right-hand side of the domain to model

wave generation only and prevent wave reflection is depicted in Figure 22b. By comparing the velocity field inside the RZ (red box), it can be noticed that the reflected waves are well absorbed. In fact, moving from the right edge of the RZ towards its center, the velocity pattern in the highly reflective case tends to the same velocity pattern as in the case where reflection is prevented. This demonstrates that the correction applied to the particle velocity as expressed by Eq.(8) and by using the weighting function defined by Eq.(10) is working properly and the target incident wave field is generated. It is worth noting that the size of the damping areas, RZ and main fluid domain in this case, has been set-up for validation purposes only, whereas for application cases the model layout has to be optimized in order to find a trade-off between RZ accuracy, model resolution and computational cost.

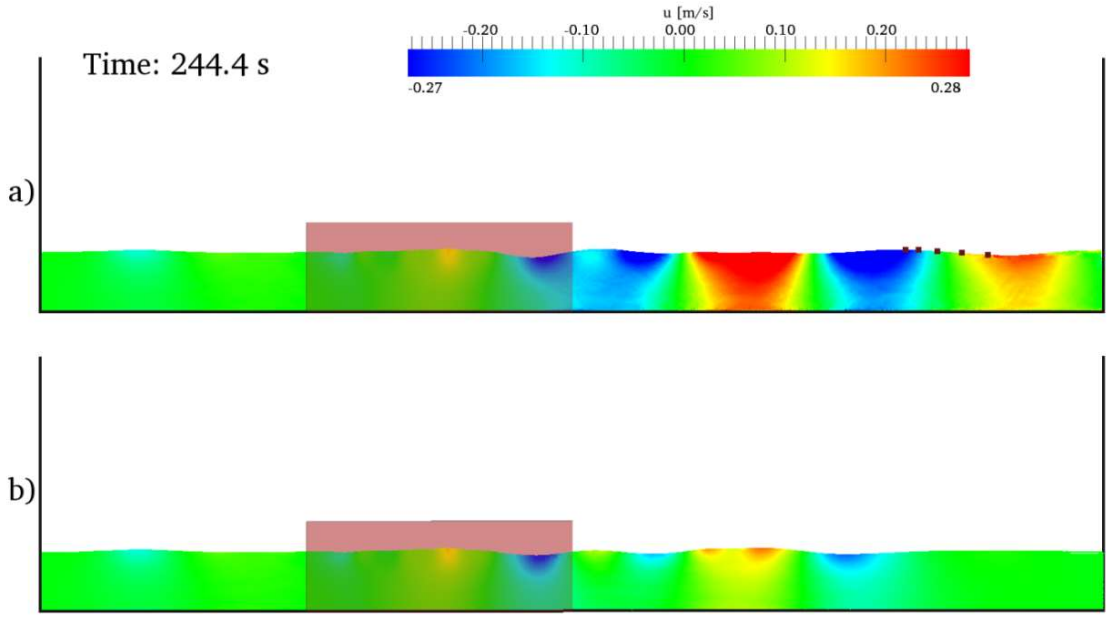

Figure 22. Snapshot of DualSPHysics simulation implementing RZ applied to couple DualSPHysics and SWASH for Case 1: horizontal velocity field in case of highly reflective conditions (a) and wave generation only (b). The red box indicates the RZ. The black dots are the five measurement points for free-surface elevation for wave reflection analysis.

Reflection analysis has been carried out using WaveLab v.3.742 from Aalborg University to separate the incident and reflected waves. The incident wave characteristics have been therefore calculated starting from the signal at the five above-mentioned measurement points. The results are reported in Table 3 together with the target wave conditions and the results from the RZ case presented in Figure 20 for wave generation only. The incident wave characteristics for the highly reflective case are almost identical to the case shown in Figure 21, that corresponds to a case with no wave refection, and they are very similar to the target wave conditions: the numerical errors are in the order of 3% for spectral wave height, peak period and spectral period. These results as the previous one for wave generation only (see Figure 21), demonstrate that the RZ, also applied for coupling width SWASH, can be extended to cases of random waves.

Table 3. Measured wave conditions for the Case 1 when RZ is applied to couple DualSPHysics and SWASH: comparison between highly reflective and generation-only case.

Setup	H_{m0} [m]		T_p [s]		$T_{m-1,0}$ [s]	$T_{m-1,0}$
Highly reflective	0.097	-2.8%	1.60	+3.2%	1.52	+3.4%
Generation only	0.096	-4.0%	1.63	+5.1%	1.54	+4.7%
Target	0.100	-	1.55	-	1.47	-

6 Case study

The coupling between SWASH and DualSPHysics by means of the RZ method is here applied to a case study consisting of wave overtopping flow impacts on sea dikes with vertical walls in shallow water conditions. RZ-SWASH is validated against experimental data for post-overtopping processes. The case of study consists of a multi-functional sea dike with gentle and very shallow foreshore [49,50]. Physical model tests were carried out in a 4.0 m wide, 1.4 m deep and 70.0 m long wave flume at Flanders Hydraulic Research, Antwerp (Belgium). The experimental campaign was carried out within the framework of the project "Hydraulic impact of overtopping waves on a multi-functional dike (1.1.1)" (UNESCO code 330506, Pr. No. 12176 -Technologiestichting STW, The Netherlands). The case study is a typical case from the Belgian and Dutch coastline, where buildings are constructed on the top of the dike. One of the major goals of the project was to characterize the forces exerted by overtopping waves on the buildings along the coastline.

The geometrical model layout is depicted in Figure 23. The model scale was 1:25. The experimental setup comprises a 1:35 foreshore slope, starting at x=13.2 m, followed by a 1:3 sloping dike with a 0.1 m height. The reference frame used in this work has the origin of x at the neutral position of the wave paddle and the origin of z is set at the bottom of the flume. A vertical wall, mimicking the presence of a building on the sea dike, was located 0.50 m landwards with respect to the crest edge of the dike.

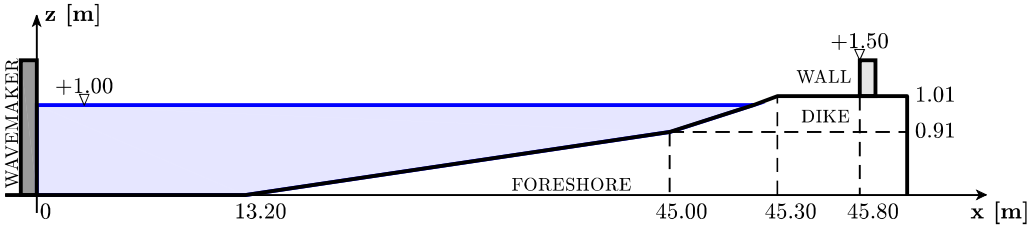

Figure 23. Layout of the physical model at FHR.

Not only forces on the vertical wall, but also layer thickness and velocity of the overtopping flows were measured. Notice that as the overtopping waves are meant those that occur at the dike crest and that can travel further up to the vertical wall. The wall is, in fact, high enough to prevent any traveling waves to go over it. A detailed analysis of the velocity field of the overtopping flows on the dike crest was carried out for regular test cases. Therefore, one regular wave case from those studied in [49] has been used for the present analysis. The wave height at the wavemaker is equal to 0.2 m, the wave period 4 s. The water depth in the flume is 1 m at the wavemaker, resulting in an offshore wavelength of 12.0 m.

6.1 Numerical modelling

The numerical modelling of the above described case study comprises a previous analysis where SWASH model has been validated against the physical model results: wave propagation, transformation and breaking have been accurately modelled and the conditions at the toe of the dike are reproduced as in the physical model test. Then SWASH has been coupled to DualSPHysics to model the wave impact. The quantities measured and compared with the experimental results are: free-surface elevation, overtopping flow thickness at three different locations along the dike crest and wave forces on the vertical wall. Both free-surface elevation and layer thickness were measured in the physical model by means of resistive wave gauges. The wave forces were measured in the physical model by means of two tension-compression load cells, model Tedea-Huntleigh 614.

A previous attempt to simulate numerically this case was presented by [51], where the hybridization technique based on MB as proposed by [14] was employed. Main limitation of this work was the incapability of the MB hybridization technique to compensate wave reflection at the MB, fact that obliged to shorten the time series with respect to the experimental one. RZ-SWASH is here proposed to overcome that limitation, while keeping the model accuracy.

The first step for the DualSPHysics-SWASH coupling applications encompasses a preliminary SWASH modelling that aims to get the incident wave conditions to be transferred from SWASH to DualSPHysics. The RZ has been located between x=22.00 m and x=26.00 m (Figure 24b). To get the incident wave conditions from SWASH at the location of RZ, it has been necessary to modify the foreshore geometry in SWASH, namely removing the foreshore after x=26.00 m, adding an horizontal bottom and sponge layer in order to get only the incident wave components in the region where the RZ is placed (Figure 24a). Thus, spurious reflected components will be prevented and only incident wave velocity information will be passed from SWASH to DualSPHysics.

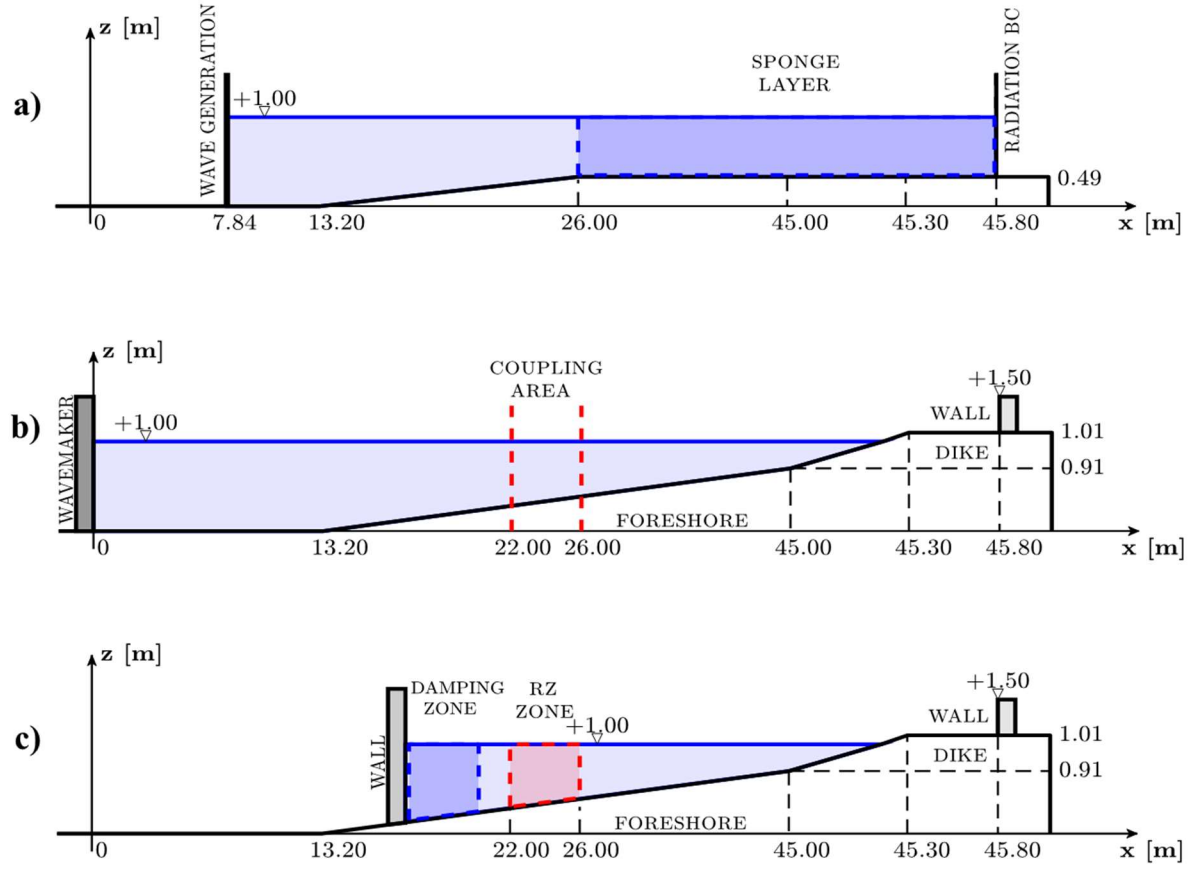

Figure 24. Layout of the flume at FHR and indication of the RZ location for the RZ-SWASH approach: a) SWASH model setup for incident wave conditions; b) coupling area location; c) couple model setup.

A sensitivity analysis on the RZ width has been performed. A width equal to 4 m that (approximately 1/3*L) has resulted accurate enough for wave generation and absorption. The hydraulic boundary conditions for DualSPHysics in the RZ has been reconstructed by interpolation of the horizontal velocity calculated at each SWASH layer. Finally, DualSPHysics has been employed to model the part of domain between the damping zone at the left-hand side of the RZ zone and the dike (Figure 24c). The optimal width of the damping zone has been assessed, being equal to L/2. The damping is located at a distance from the left-hand edge of the RZ equal to L/8. An initial interparticle distance dp=0.003 m has been used leading to 1,269,820 SPH fluid particles. Sixty seconds of physical time have been simulated in the TITAN X graphic card, taking 27.2 h.

The numerical and experimental free-surface elevation, layer thickness and wave forces exerted on the vertical wall are plotted in Figure 25, showing that the numerical solution resembles the experimental accurately. The differences that still exist between numerical model and the experiments can be partly explained because of the highly turbulent and stochastic nature of the overtopping wave impact, that makes the experimental test not repeatable and not strictly two-dimensional (the wave front after breaking

is not completely perpendicular to the direction of the wave propagation). Refer to [52] for further discussions on model inaccuracy and effect of non-repeatability on wave impact modelling. Some re-reflection pattern is noticed very close to the wall. Some numerical reflection might be noticed, which increases the magnitude of the last two impacts with respect to the experimental results. Besides, a certain asymmetry of the free-surface elevation, specifically related to the wave trough, is noticeable in Figure 25a. It is worth to remember that the RZ is located close to the breaking zone, facts that might induce unwanted non-linear effects. Further optimization of the RZ setup for very shallow water cases with heavy wave breaking can smooth this difference. This optimization is not performed for the present work. Yet, the results demonstrate that the application of RZ-SWASH allows shortening the SPH domain and improving model efficiency. To run the same model by employing DualSPHysics as stand-alone model and using the same model resolution would require 114.7 h (≈5 days) for 3,389,266 fluid particles. The results of employing DualSPHysics as stand-alone model to reproduce the case study are reported in [48] and are omitted here for sake of simplicity. Here we want to stress that a significant reduction in the computation time is achieved by using RZ-SWASH. However, one has to remind that the reduction is case-dependent: the closer is the RZ to the analyzed structure the smaller is the SPH domain, resulting in a faster model execution. In the presented case a speed-up of 4.2 times has been attained.

Finally the horizontal velocity field on the dike crest and close to the vertical wall is depicted in Figure 26 for the RZ-SWASH case. The experimental velocity was reconstructed employing a Bubble Image Velocimetry technique (BIV). The analyzed area corresponded to the last 50 cm of dike crest, close to the wall. Experimental and numerical velocity magnitude are plotted using the same color gradient in Figure 26. The snapshots correspond to t=45.95 s, time when, after an initial impact, the following fluid wedge has risen up the face of the wall, reached the maximum run-up height and is started to be reflected back. During this stage, the momentum of the fluid flow is inverted due to the flow deflection. This can be noticed looking at the negative (i.e. oriented seawards) horizontal velocity that characterizes the fluid flow close to the vertical wall. Notice that the generated overtopping flow on the dike is a highly aerated flow, due to the wave breaking processes that occur on the foreshore before the dike. Nevertheless, only the fluid phase is modelled with DualSPHysics at the present stage. The absence of the air-phase in the numerical model can therefore explain the slight differences between numerical and experimental results. Yet, the numerical model provides results in agreement with the physical model tests.

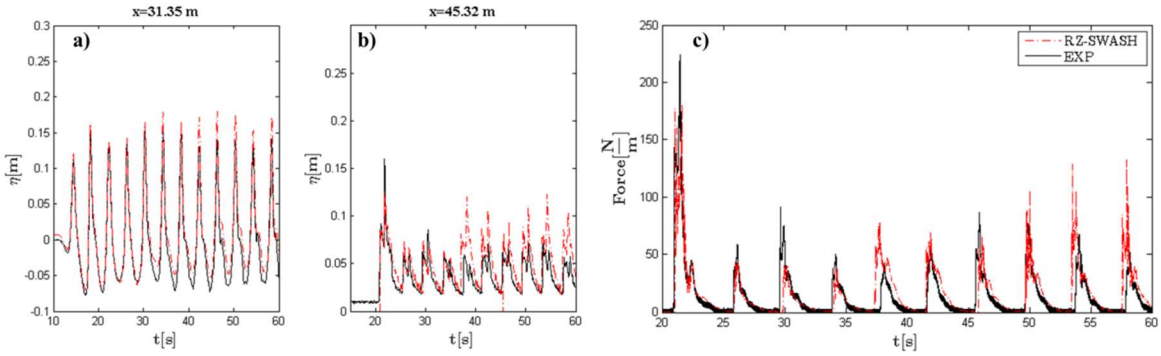

Figure 25. Results of water-surface elevation (a), overtopping layer thickness (b) and wave force (c) using RZ-SWASH: numerical (red dahs-dot line) vs experimental (black solid line)

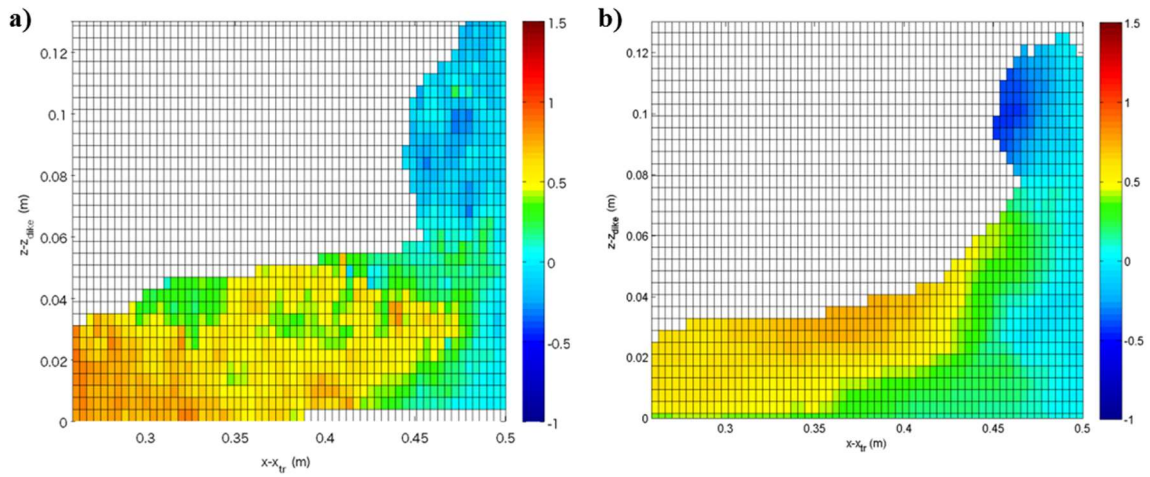

Figure 26. Results of horizontal velocity field on the dike crest using RZ-SWASH at t=45.95 s: experimental (a) vs numerical (b)

7 Conclusions

Relaxation Zone (RZ) technique has been implemented in DualSPHysics and tested the performance of wave generation and wave reflection compensation for 2nd-order Stokes' waves. In order to optimize the performance of RZ, an hyperbolic C function which generalizes and extends the one proposed by [30] is implemented. The model performance of RZ depends on the shape of the C function and the parameters related to the width of the RZ. The optimum values for RZ width and the ψ and β parameters that define the C function are determined through more than 2,000 simulations for both wave generation and wave reflection compensation. Ten different regular wave cases have been simulated, covering a wide steepness range between 1.08% and 3.52%. To assess the accuracy for wave generation only, damping areas are introduced in the SPH domain, in order to avoid any re-reflection towards the RZ. Meanwhile, to analyze the response of the RZ to reflected waves, the SPH domain comprises a fully-reflective vertical wall, which represents the most critical layout for wave reflection compensation. Overall the new RZ technique shows a very good performance in wave generation. It has been proven that the performance depends on the correlation between the generation width and the shape of the C function and a method to design the RZ has been presented. It is also demonstrated that the influence of the width of the RZ decreases as the wave steepness decreases, being the numerical error almost independent on the RZ width for very low steepness values, namely around 1%. For wave reflection, a first transitional phase is present in the free-surface elevation, which requires a few waves to be dissipated, with consequent extra computational cost due to the need to generate longer wave trains in order to achieve a stable solution. However, after the transitional phase, the reflected waves are properly absorbed by the RZ. A method to design the RZ in case of highly-reflective cases is also proposed.

Then, the RZ is extended to couple DualSPHysics model to the wave propagation model SWASH (RZ-SWASH), proving similar accuracy as the RZ as stand-alone method. Finally, the new technique is extended to irregular wave cases for the generation of real sea states. The new RZ-SWASH method has been tested and compared also with physical model results for post-overtopping processes on sea dikes. Despite some model inaccuracies that can be solved by further optimization of the RZ setup, it can be concluded that RZ-SWASH allows reducing significantly the computational time, four times smaller than the DualSPHysics stand-alone model for the case here investigated, and provides reasonable results in terms of wave transformation in a shallow foreshore, overtopping flow velocities and wave force on a vertical wall on a dike.

All results indicate that the Relaxation Zone technique can be one of the important alternative for wave generation in SPH-based model for coastal engineering application. It is worthy to remind here the implementation of RZ does not aim at replacing the most classical Moving Boundary (MB) generation technique in DualSPHysics. It is always preferable use MB in case of deep and intermediate water and

when the numerical domain is not so extensive so that the computation can be performed at affordable costs and time. However, there are critical cases in coastal engineering where using MB would require to model very large domains to ease the processes of wave transformation and breaking, wave-wave interaction, release of bound wave components, energy wave spreading, etc. In those cases, it would be better to move towards the coastline the zone where in the model the waves are generated. To do that, alternative generation techniques are required, where MB fails or become inaccurate. RZ is one of those technique, especially because it is meant to link DualSPHysics with a faster and cheaper wave propagation model, like SWASH.

Acknowledgements

We thank Prof. S. Aoki from Osaka University, Japan to promote the internship at Flanders Hydraulics Research of Akihiro Usui, who contributed to develop the hyperbolic weighting function that has been implemented in DualSPHysics. The physical model tests carried out at Flanders Hydraulics Research were sponsored by the STW-programme on integral and sustainable design of multifunctional flood defences, Project No. 12760, Flanders Hydraulic Research, and the WTI 2017 project (1209437) (Research and development of safety assessment tools of Dutch flood defences), commissioned by the department WVL of Rijkswaterstaat in the Netherlands. This work was partially financed by Xunta de Galicia (Spain) under project ED431C 2017/64 "Programa de Consolidación e Estructuración de Unidades de Investigación Competitivas (Grupos de Referencia Competitiva)" cofunded by European Regional Development Fund (FEDER). The work is also funded by the Ministry of Economy and Competitiveness of the Government of Spain under project "WELCOME ENE2016-75074-C2-1-R".

References

[1] H. Gotoh, A. Khayyer, On the state-of-the-art of particle methods for coastal and ocean engineering, Coast. Eng. J. 0 (2018) 1–25. doi:10.1080/21664250.2018.1436243.

[2] J.J. Monaghan, Smoothed particle hydrodynamics, Reports Prog. Phys. 68 (2005) 1703–1759. doi:10.1088/0034-4885/68/8/R01.

[3] D. Violeau, Fluid Mechanics and the SPH Method: Theory and Applications, 2012.

[4] B.D. Rogers, R.A. Dalrymple, P.K. Stansby, Simulation of caisson breakwater movement using 2-D SPH, J. Hydraul. Res. 48 (2010) 135–141. doi:10.1080/00221686.2010.9641254.

[5] J.L. Lara, N. Garcia, I.J. Losada, RANS modelling applied to random wave interaction with submerged permeable structures, 53 (2006) 395–417. doi:10.1016/j.coastaleng.2005.11.003.

[6] A.J.C. Crespo, J.M. Domínguez, B.D. Rogers, M. Gómez-Gesteira, S. Longshaw, R. Canelas, R. Vacondio, A. Barreiro, O. García-Feal, DualSPHysics: Open-source parallel CFD solver based on Smoothed Particle Hydrodynamics (SPH), Comput. Phys. Commun. 187 (2015) 204–216. doi:10.1016/j.cpc.2014.10.004.

[7] J.M. Domínguez, A.J.C. Crespo, D. Valdez-Balderas, B.D. Rogers, M. Gómez-Gesteira, New multi-GPU implementation for smoothed particle hydrodynamics on heterogeneous clusters, Comput. Phys. Commun. 184 (2013) 1848–1860. doi:10.1016/J.CPC.2013.03.008.

[8] C. Altomare, G. Viccione, B. Tagliafierro, V. Bovolin, J.M. Domínguez, A.J.C. Crespo, Free-Surface Flow Simulations with Smoothed Particle Hydrodynamics Method using High-Performance Computing, in: A. Ionescu (Ed.), Comput. Fluid Dyn. - Basic Instruments Appl. Sci., InTech, Rijeka, 2018. doi:10.5772/intechopen.71362.

[9] M. Narayanaswamy, A. Jacobo, C. Crespo, R.A. Dalrymple, SPHysics-FUNWAVE hybrid model for coastal wave propagation SPHysics-FUNWAVE hybrid model for coastal wave propagation Modèle hybride SPHysics-FUNWAVE pour la propagation côtière des vagues, 1686 (2017). doi:10.3826/jhr.2010.0007.

[10] C. Altomare, A.J.C. Crespo, J.M. Domínguez, M. Gómez-Gesteira, T. Suzuki, T. Verwaest, Applicability of Smoothed Particle Hydrodynamics for estimation of sea wave impact on coastal structures, Coast. Eng. 96 (2015) 1–12. doi:10.1016/j.coastaleng.2014.11.001.

[11] P. St-germain, I. Nistor, M. Asce, R. Townsend, T. Shibayama, Smoothed-Particle Hydrodynamics Numerical Modeling of Structures Impacted by Tsunami Bores, 1 (2014) 66–81. doi:10.1061/(ASCE)WW.1943-5460.0000225.

[12] G. Fourtakas, P.K. Stansby, B.D. Rogers, S.J. Lind, An Eulerian–Lagrangian incompressible SPH formulation (ELI-SPH) connected with a sharp interface, Comput. Methods Appl. Mech. Eng. 329 (2018) 532–552. doi:10.1016/J.CMA.2017.09.029.

[13] S. Marrone, A. Di Mascio, D. Le Touzé, Coupling of Smoothed Particle Hydrodynamics with Finite Volume method for free-surface flows, J. Comput. Phys. 310 (2016) 161–180. doi:10.1016/J.JCP.2015.11.059.

[14] C. Altomare, J.M. Domínguez, a J.C. Crespo, T. Suzuki, I. Caceres, M. Gómez-Gesteira, Hybridization of the Wave Propagation Model SWASH and the Meshfree Particle Method SPH for Real Coastal Applications, Coast. Eng. J. 57 (2015) 1550024. doi:doi:10.1142/S0578563415500242.

[15] T. Verbrugghe, J.M. Domínguez, A.J.C. Crespo, C. Altomare, V. Stratigaki, P. Troch, A. Kortenhaus, Coupling methodology for smoothed particle hydrodynamics modelling of non-linear wave-structure interactions, Coast. Eng. 138 (2018) 184–198. doi:10.1016/j.coastaleng.2018.04.021.

[16] C. Altomare, J.M. Domínguez, A.J.C. Crespo, J. González-Cao, T. Suzuki, M. Gómez-Gesteira, P. Troch., Long-crested wave generation and absorption for SPH-based DualSPHysics model, Coast. Eng. 127 (2017) 37–54. doi:10.1016/j.coastaleng.2017.06.004.

[17] H.A. Schaffer, G. Klopman, Review of multidirectional active wave absorption methods, J. Waterw. Port, Coast. Ocean Eng. 126 (2000) 88–97.

[18] C. Altomare, T. Suzuki, X. Chen, T. Verwaest, A. Kortenhaus, Wave overtopping of sea dikes with very shallow foreshores, Coast. Eng. 116 (2016). doi:10.1016/j.coastaleng.2016.07.002.

[19] T. Suzuki, C. Altomare, W. Veale, T. Verwaest, K. Trouw, P. Troch, M. Zijlema, Efficient and robust wave overtopping estimation for impermeable coastal structures in shallow foreshores using SWASH, Coast. Eng. 122 (2017) 108–123. doi:10.1016/j.coastaleng.2017.01.009.

[20] P. Higuera, I.J. Losada, J.L. Lara, Three-dimensional numerical wave generation with moving boundaries, Coast. Eng. 101 (2015) 35–47. doi:10.1016/j.coastaleng.2015.04.003.

[21] H. Wen, B. Ren, P. Dong, Y. Wang, A SPH numerical wave basin for modeling wave-structure interactions, Appl. Ocean Res. 59 (2016) 366–377. doi:10.1016/J.APOR.2016.06.012.

[22] P. Troch, J. De Rouck, An active wave generating – absorbing boundary condition for VOF type numerical model, (1999).

[23] P. Higuera, J.L. Lara, I.J. Losada, Realistic wave generation and active wave absorption for Navier-Stokes models. Application to OpenFOAM®., Coast. Eng. 71 (2013) 102–118. doi:10.1016/j.coastaleng.2012.07.002.

[24] M. Zijlema, G. Stelling, P. Smit, SWASH: An operational public domain code for simulating wave fields and rapidly varied flows in coastal waters, Coast. Eng. 58 (2011) 992–1012. doi:10.1016/j.coastaleng.2011.05.015.

[25] G. Wei, J.T. Kirby, Time-Dependent Numerical Code for Extended Boussinesq Equations, 121 (1995) 251–261.

[26] P. Lin, P.L.-F. Liu, Internal Wave-Maker for Navier-Stokes Equations Models, J. Waterw. Port Coast. Ocean Eng. 125 (1999) 207–215.

[27] H.A. Schäffer, O.R. Sørensen, On the internal wave generation in Boussinesq and mild-slope equations, Coast. Eng. 53 (2006) 319–323. doi:10.1016/j.coastaleng.2005.10.022.

[28] X. Liu, P. Lin, S. Shao, ISPH wave simulation by using an internal wave maker, Coast. Eng. 95 (2015) 160–170. doi:10.1016/j.coastaleng.2014.10.007.

[29] H. Wen, B. Ren, A non-reflective spectral wave maker for SPH modeling of nonlinear wave motion, Wave Motion. 79 (2018) 112–128. doi:10.1016/J.WAVEMOTI.2018.03.003.

[30] X. Ni, W.B. Feng, Numerical Simulation of Wave Overtopping Based on DualSPHysics Xingye Ni 1, 408 (2013) 1463–1471. doi:10.4028/www.scientific.net/AMM.405-408.1463.

[31] E.Y.M. Lo, S. Shao, Simulation of near-shore solitary wave mechanics by an incompressible SPH method, Appl. Ocean Res. 24 (2002) 275–286.

[32] M. Brorsen, J. Larsen, Source Generation of Nonlinear Gravity Waves with the Boundary Integral Equation Method, Coast. Eng. 11 (1987) 93–113.

[33] R. Vacondio, B.D. Rogers, P.K. Stansby, P. Mignosa, SPH Modeling of Shallow Flow with Open Boundaries for Practical Flood Simulation, J. Hydraul. Eng. 138 (2012) 530–541. doi:10.1061/(ASCE)HY.1943-7900.0000543.

[34] Leroy, Violeau, Ferr, Fratter, Joly, A new open boundary formulation for incompressible SPH, Comput. Math. with Appl. 72 (2016) 2417–2432. doi:10.1016/j.camwa.2016.09.008.

[35] X. Ni, W. Feng, S. Huang, Y. Zhang, X. Feng, A SPH numerical wave flume with non-reflective open boundary conditions, Ocean Eng. 163 (2018) 483–501. doi:10.1016/J.OCEANENG.2018.06.034.

[36] E. Pugliese Carratelli, G. Viccione, V. Bovolin, Free surface flow impact on a vertical wall: a numerical assessment, Theor. Comput. Fluid Dyn. 30 (2016) 403–414. doi:10.1007/s00162-016-0386-9.

[37] A.J.C. Crespo, J.M. Dominguez, A. Barreiro, M. Gómez-Gesteira, B.D. Rogers, GPUs, a new tool of acceleration in CFD: efficiency and reliability on smoothed particle hydrodynamics methods., PLoS One. 6 (2011) e20685. doi:10.1371/journal.pone.0020685.

[38] A.J.C. Crespo, C. Altomare, J.M. Domínguez, J. González-Cao, M. Gómez-Gesteira, Towards simulating floating offshore oscillating water column converters with Smoothed Particle Hydrodynamics, Coast. Eng. 126 (2017) 11–26. doi:10.1016/J.COASTALENG.2017.05.001.

[39] F. Zhang, A. Crespo, C. Altomare, J. Domínguez, A. Marzeddu, S. Shang, M. Gómez-Gesteira, DualSPHysics: A numerical tool to simulate real breakwaters, J. Hydrodyn. 30 (2018) 95–105. doi:10.1007/s42241-018-0010-0.

[40] C. Altomare, A.J.C. Crespo, B.D. Rogers, J.M. Dominguez, X. Gironella, M. Gómez-Gesteira, Numerical modelling of armour block sea breakwater with smoothed particle hydrodynamics, Comput. Struct. 130 (2014) 34–45. doi:10.1016/j.compstruc.2013.10.011.

[41] J.J. Monaghan, Smoothed particle hydrodynamics, Annu. Rev. Astron. Astrophys. 30 (1992) 543–574.

[42] H. Wendland, Piecewise polynomial, positive definite and compactly supported radial functions of minimal degree, Adv. Comput. Math. 4 (1995) 389–396. doi:10.1007/BF02123482.

[43] M. Antuono, A. Colagrossi, S. Marrone, D. Molteni, Free-surface flows solved by means of SPH schemes with numerical diffusive terms, Comput. Phys. Commun. 181 (2010) 532–549. doi:10.1016/j.cpc.2009.11.002.

[44] R.A. Rota Roselli, G. Vernengo, C. Altomare, S. Brizzolara, L. Bonfiglio, R. Guercio, Ensuring numerical stability of wave propagation by tuning model parameters using genetic algorithms and response surface methods, Environ. Model. Softw. 103 (2018) 62–73.

doi:10.1016/j.envsoft.2018.02.003.

[45] A.J.C. Crespo, M. Gómez-Gesteira, R. Dalrymple, Boundary Conditions Generated by Dynamic Particles in SPH Methods, Comput. Mater. Contin. 5 (2007) 173–184. citeulike-article-id:3478400.

[46] M. Zijlema, G. Stelling, P. Smit, SWASH : An operational public domain code for simulating wave fi elds and rapidly varied fl ows in coastal waters, Coast. Eng. 58 (2011) 992–1012. doi:10.1016/j.coastaleng.2011.05.015.

[47] N.G. Jacobsen, D.R. Fuhrman, J. Fredsøe, A wave generation toolbox for the open-source CFD library: OpenFoam®, Int. J. Numer. Methods Fluids. 70 (2012) 1073–1088. doi:10.1002/fld.2726.

[48] C. Altomare, B. Tagliafierro, T. Suzuki, J.M. Dominguez, A.J.C. Crespo, R. Briganti, Relaxation zone method in SPH-based model applied to wave-structure interaction, in: Int. Ocean Polar Eng. Conf., Sapporo, 2018: pp. 627–634.

[49] X. Chen, B. Hofland, C. Altomare, T. Suzuki, W. Uijttewaal, Forces on a vertical wall on a dike crest due to overtopping flow, Coast. Eng. 95 (2015) 94–104. doi:10.1016/j.coastaleng.2014.10.002.

[50] X. Chen, B. Hofland, W. Uijttewaal, Maximum overtopping forces on a dike-mounted wall with a shallow foreshore, Coast. Eng. 116 (2016) 89–102. doi:10.1016/j.coastaleng.2016.06.004.

[51] T. Altomare, C; Oshima, Y; Chen, X; Crespo, A.J.C.; Suzuki, Study of the overtopping flow impacts on multifunctional sea dikes in shallow foreshores with an hybrid numerical model, E-Proceedings 36th IAHR World Congr. 28 June – 3 July, 2015, Hague, Netherlands. (2015) 1–11.

[52] D. Kisacik, P. Troch, P. Van Bogaert, Description of loading conditions due to violent wave impacts on a vertical structure with an overhanging horizontal cantilever slab, Coast. Eng. 60 (2012) 201–226. doi:10.1016/j.coastaleng.2011.10.001.

List of figures

List of Tables